Permafrost and Periglacial Processes

WILEY

RESEARCH ARTICLE OPEN ACCESS

Evaluating Testability of Permafrost Models Through Physical and Thermal Testing in Complex Mountain Terrain, Yukon, Canada

Ria Nicholson[1] | Philip P. Bonnaventure[1] | Nick C. Noad[1] | Madeleine C. Garibaldi[1] | Rabecca Thiessen[1] | Will Kochtitzky[2]

[1]Department of Geography and Environment, University of Lethbridge, Lethbridge, Alberta, Canada | [2]School of Marine and Environmental Programs, University of New England, Biddeford, Maine, USA

Correspondence: Ria Nicholson (maria.nicholson@uleth.ca)

Received: 6 August 2025 | **Revised:** 27 May 2026 | **Accepted:** 2 June 2026

Keywords: Dempster Highway | ground thermal profiling | ground truthing | permafrost | permafrost model validation | thermal heterogeneity | Yukon

ABSTRACT

Due to its subsurface nature, permafrost cannot be directly observed with the naked eye or optical remote sensing. Consequently, accurately describing its distribution and thermal state is challenging. This is especially true in vast, remote environments, where obtaining comprehensive field data is demanding or improbable. This results in a reliance on models, which are constrained by limited, spatiotemporally fragmented baseline data, and which are rarely validated against actual field data. While such models may be sufficient in homogeneous permafrost environments, or to capture general trends over large areas, their accuracy is limited at finer scales in thermally heterogeneous environments. To explore and conceptualize this issue, we conducted a field sampling campaign in two thermally complex valleys in the Ogilvie Mountains. The study area exhibits strong ground temperature variability over short distances due to surface-based temperature inversions, extreme aspects, and complex land cover types. Our objective was to qualitatively assess our ability to collect in situ permafrost thermal data ("testability") using simple, repeatable, low-cost methods. Although the study area is located within the zone of continuous permafrost, only nine (18.3%) of the 49 Cryotic Assessment Sites (CAS) produced cryotic temperatures in situ, due to substrate clast density and active layer thickness. Testability outcomes were used to develop a generalized linear model (P_{TEST}), which predicts low testability at higher elevations and higher testability in valley bottoms, indicating a substantial potential sampling bias for model calibration and validation. Comparisons with two local permafrost models highlight persistent uncertainty in permafrost characterization in mountainous environments.

1 | Introduction

It is widely accepted that permafrost thaw is being driven by anthropogenic climate change (i.e., [1, 2]), with increased warming occurring in the circumpolar Arctic [3] and in mountainous regions [4, 5]. The resultant permafrost degradation has made significant contributions to greenhouse gas emissions [6], decreased the stability of critical infrastructure [7, 8], and jeopardized the security of food and drinking water in northern communities [9]. In mountainous permafrost environments, there is also an increased risk of destructive slope processes, such as active layer detachments and retrogressive thaw slumps [10, 11]. However, monitoring these issues is challenging because of uncertainties surrounding permafrost distribution and ground thermal state in thermally heterogeneous zones.

Permafrost is a subsurface, temporal, thermally defined phenomenon [12], which makes it challenging to observe directly

and consistently. Unlike sea ice and glaciers, permafrost cannot be directly observed using the human eye or optical remote sensing [13–16]. Although permafrost is estimated to underlie approximately 15%–24% of the Earth's terrestrial surface [17, 18], delineating specific "boundaries" of permafrost is difficult because it is an attempt to map a condition, not a substance [19]. Although numerous models have been developed to map permafrost presence on local, regional, and global scales (e.g., [17, 20–22]) comparatively few are trained on comprehensive in situ thermal state data sets or undergo any kind of field validation. This is problematic because models can only be as accurate as the parameters constraining them, and the ability to validate permafrost spatial distribution is necessary for model input [23, 24]. However, there is no method to directly map permafrost on large scales at resolutions, which are sufficient to detect change [25], and in situ observations of permafrost spatiotemporal data are highly spatiotemporally fragmented. This lack of data increases uncertainty regarding both extent and ground thermal state [26, 27].

Uncertainty about permafrost distribution and thermal state is especially pronounced in mountainous environments, where greater thermal heterogeneity is caused by extreme aspects, elevational cooling or surface-based temperature inversions (SBIs), snow cover, and substrate [23, 28–30]. Boreholes can be used in mountains to provide valuable, consistent data on long timescales, but there are only limited guidelines available for their installation [31] and deploying them is difficult due to remoteness, operational difficulties, and cost [32]. Furthermore, boreholes also only provide data about a discrete point in the landscape, which is not likely to be sufficient to describe change in zones of high thermal heterogeneity (e.g., [33]).

Thermal heterogeneity refers to variations in surface energy balance caused by topography, vegetation, snow depth, and soil texture, which create localized variations in permafrost distribution [24, 34, 35]. This phenomenon is most prominent in the extensive-discontinuous zone [36] and in mountainous regions [23], but can still occur in cold, high latitude environments, which are typically assumed to be underlain by continuous permafrost [37]. These patterns of spatial and thermal heterogeneity are too fine to be captured by current global scale models [23, 36, 38]. One such example of this is the general circulation models (GCMs) used by the IPCC to forecast global response to climate change (e.g., CMIP5 and CMIP6), which operate on scales of 100–300 km [39]. This uncertainty has significant implications for infrastructure planning and adaptation [40] and for predicting ecological responses to change [38].

Many permafrost environments are vast, highly remote, and potentially hazardous. In some cases, they may only be accessible on foot or by helicopter or have steep unstable slopes. Mountainous environments are exemplary of this, and the ability of researchers to obtain samples is restricted by physical fitness and safety issues. Furthermore, the substrate overlying permafrost may simply be impenetrable to hand-operated probes, such as in rocky polar deserts, felsenmeer, or other clast-rich substrates. It may also be the case that instrument penetration is possible, but only to limited depths, which are not sufficient to reach the bottom of the active layer.

This study is an attempt to conceptualize the issue of "permafrost testability," which is the ability of a researcher to obtain in situ permafrost thermal data using simple, repeatable, low-cost methods in a complex environment. To do this, we conducted a field campaign during which we attempted to obtain permafrost data from several Cryotic Assessment Sites (CAS) in two proximal valleys in the Ogilvie Mountains. The goal of this field campaign was not to determine actual permafrost distribution in thermal state, but to qualitatively assess our ability to do so, a critical step in model validation.

2 | Study Area

This research was conducted in a subrange of the Ogilvie Mountains, located in the north-central Yukon along the Dempster Highway (Figure 1). The Dempster Highway is of special concern for permafrost monitoring because it is the only all-season artery of transportation in the Canadian northwestern Arctic, with 90% of its 738-km length built over continuous permafrost [7]. Ongoing impacts of climate change, and the impacts of the infrastructure itself, are expected to increase active layer thicknesses (ALTs) and embankment subsidence [41].

The study area is classified as sub-Arctic, with short, cool summers and long, cold winters (Dfc) according to the Köppen-Geiger climate index [42]. It is dominated by alpine-tundra vegetation [43]. The nearest Environment Canada climate station is located approximately 160 km southwest in Dawson City. Climate normals (1991–2020) from this station report seasonal average temperatures ranging from −26.0°C to 15.7°C and approximately 360 mm of annual precipitation, with 43% falling as snow (Environment Canada, 2023). However, Dawson City is located at a significantly lower elevation (320 meters above sea level) [44] than the Ogilvie Mountains. The nearest Global Terrestrial Network for Permafrost (GTN-P) active layer monitoring station is also located in Dawson City (see [45]) and the nearest active permafrost borehole is in Red Creek valley (10 km north) [46, 47].

The subrange of interest in the Ogilvie Mountains is characterized by narrow colluvium walls and intense cold-air drainage [48] with elevations ranging from 250 to 1835 m asl (Yukon Ecoregions Working Group 2004, [7, 49]). This region has not been glaciated since the Mid-Pleistocene (2.6 Ma to > 200 Ka), leaving it uninsulated from the cold air of the Last Glacial Maximum [50, 51]. Resultant in situ bedrock weathering of the mountainous landscape resulted in periglacial facies, also known as felsenmeer [52], across the study area.

The study was conducted in two mountain valleys adjacent to the Dempster Highway due to the presence of an existing comprehensive network of air and ground temperature sensors. The network includes ground temperature nodes (GTNs) and air temperature sensors along elevational transects to monitor SBIs and their impacts on permafrost distribution (see [30, 48, 49, 53, 54]). This network is a key portion of evidence, as very few networks like it exist to provide consistent long series ground surface temperature (GST) values or data about GST spatiotemporal heterogeneity [55]. The area has also been the site of recent air, ground surface, and permafrost distribution modeling using the temperature at the top of permafrost (TTOP) modeling method [30, 53].

Heginbottom et al. [56] classified the area as having extensive-continuous permafrost (50%–90% permafrost coverage) with medium to low ground ice content (< 10%–20%). O'Neill et al. [57] also mapped the area to have negligible ground ice. Probability modeling done by Bonnaventure et al. [58] saw permafrost probabilities decreasing at middle elevations, particularly on south-facing slopes, and increasing at high elevations and in valley bottoms as a response to the presence of SBIs [53, 59]. Other studies have also assessed permafrost conditions at different points along the Dempster Highway and the surrounding area (e.g., [43, 60, 61]).

For the purposes of this study, the southern valley is called Weather Station Valley 01 (WS01; unofficial name; 64°57′N, −138°16′W) and the northern valley is called Weather Station Valley 02 (WS02; unofficial name; 65°02′N, −138°16′W; Figure 1). The valleys are located approximately 10 km apart, with dissimilarities of orientation, vegetation type and coverage, fetch length, and geometry [48, 49, 54]. On average, WS02 is 100 m higher than WS01. Although permafrost is estimated to be continuous in this region [56, 62], recent localized studies [53] have modeled more heterogeneous permafrost distribution within the valleys, especially in WS01.

Forest cover is largely coniferous and dominated by black spruce (*Picea mariana*). Other vegetation species observed include Labrador tea (*Rhododendron groenlandicum*), field horsetail (*Equisetum arvense*), dwarf birch shrubs (*Betula nana*), and net-leaved willow shrubs (*Salix reticulata*).

WS01 (Figure 2A) is a V-shaped, eastern-facing mountain valley bisected by a creek with a fetch length of 5.3 km. Average annual mean air temperature (AMAT) for the WS01 valley is modeled to be −6.4°C (2019–2021; [53]). The south-facing slope is forested,

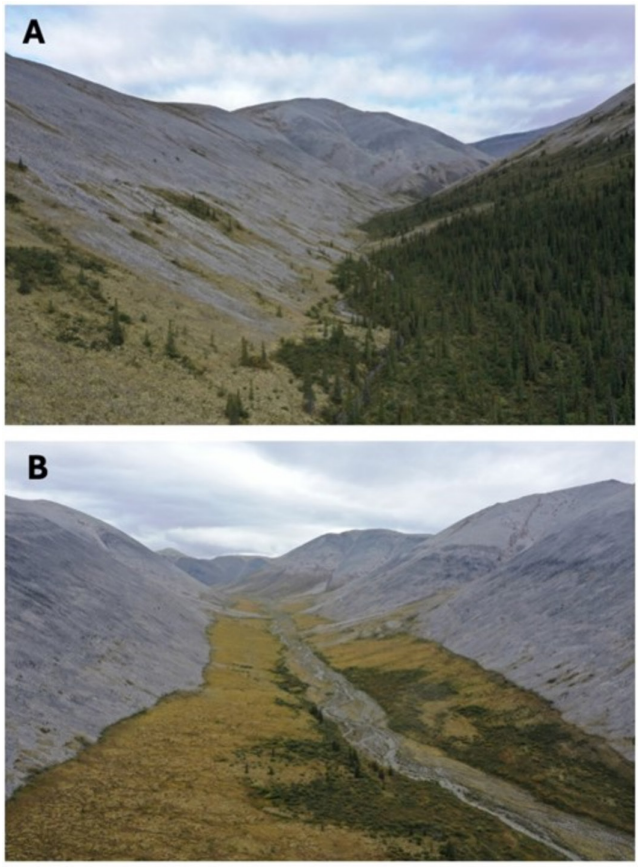

FIGURE 2 | Aerial imagery of WS01 (A) facing eastwards down the valley fetch, and WS02 (B) facing southwards down the valley fetch produced by a drone in the study area in August 2023. Image by P.P. Bonnaventure. [Colour figure can be viewed at wileyonlinelibrary.com]

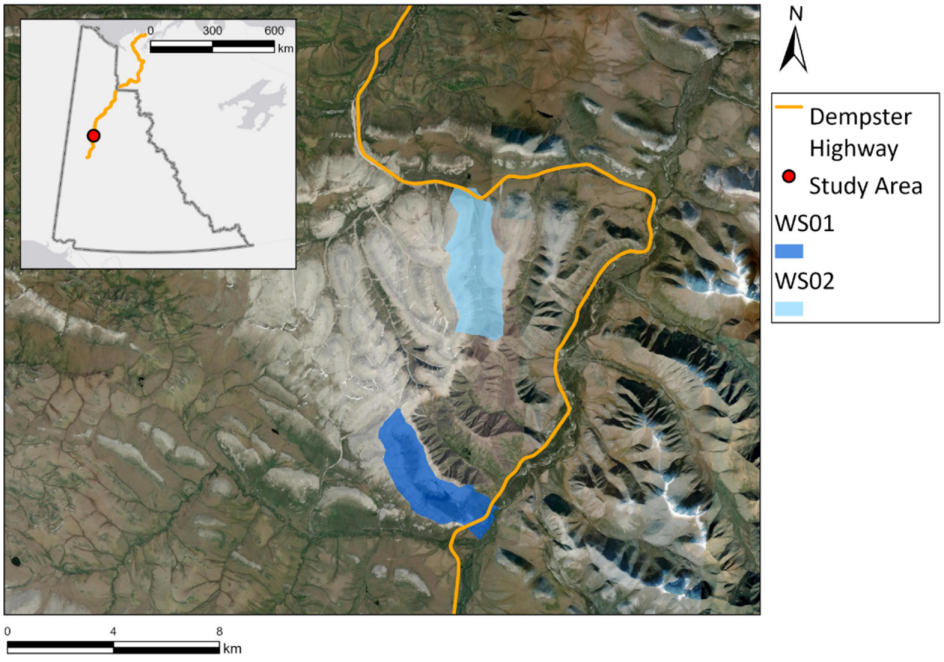

FIGURE 1 | A map of the study area, displayed on the local scale of the Ogilvie Subrange (right) and in the larger Yukon Territory (left). Basemap imagery provided by ESRI (2025). [Colour figure can be viewed at wileyonlinelibrary.com]

with vegetation prominently featuring black spruce and variable thickness *Sphagnum* spp. mosses growing over felsenmeer. The north-facing slope is un-treed felsenmeer, sparsely vegetated with some soil development in eroded drainage channels on the slope. Per a supervised land cover classification (not pictured), WS01 is overlain by 59.1% felsenmeer, 25.7% herbaceous, and 15.2% forest.

WS02 (Figure 2B) is a U-shaped valley with a north-facing orientation and a 4.7-km fetch length. Despite its proximity to WS01, it differs considerably in terms of vegetation. A small number of trees are present near the road and cluster around the creek, which bisects the fetch at the mouth of the valley but are otherwise absent. Instead, the valley floor is thickly vegetated by *Sphagnum* spp. mosses and grassy hummocks. Average AMAT for the WS02 valley was modeled to be −5.1°C (2019–2021; [53]). The land cover classification indicates WS02 is covered by 68.8% felsenmeer, 28.2% herbaceous, and 3.0% forest.

3 | Methods

3.1 | Temperature Network

Since 2017, WS01 and WS02 have been equipped with an annually expanding network of air and ground temperature sensors. The network includes several elevational transects of over 100 GTNs, more than 50 air temperature stations, and two main weather stations (HOBO USB Micro Station Data Loggers, accurate within ±0.25°C). The weather stations record wind speed and direction, atmospheric and relative humidity, incoming solar radiation, air temperature, and GST. Most sites are GTN-only, but each air temperature sensor is also associated with a GTN. Each GTN is buried approximately 2–5 cm below the surface [63] and sensors log every 2 h. Data retrieval occurs annually in August, on foot. All mean annual air temperature (MAAT) and mean annual ground surface temperature (MAGST) data used in this study were obtained from these sensors.

3.2 | Cryotic Assessment Site Selection

CAS (Table 1) were selected from pre-existing GTN locations in both valleys so that available MAGST could be used as supporting evidence for permafrost presence or absence. In a small number of cases, additional CAS without GTN were added where they represented key thaw features. MAGST was not available at these sites.

During the initial assessment of CAS, MAGST ≤ 0°C was taken to indicate likely permafrost presence and MAGST ≥ 1°C likely absence. However, at some CAS, environmental conditions suggested the potential for ecosystem-protected permafrost (e.g., thick organic mats, moss cover, and shading), where permafrost may persist even when MAGST slightly exceeds 0°C [35, 64]. Because no universally accepted upper MAGST limit for permafrost exists, we defined a conservative near-thaw sensitivity range for sites with MAGST between 0.1°C and 0.9°C in settings where ecosystem-protected permafrost was plausible. These MAGST-based categories are used only as an operational site-level framework, based on measured GSTs and local land cover, to distinguish likely permafrost presence, likely absence, and sites where near-surface thermal conditions are close enough to the threshold that permafrost occurrence remains difficult to assess confidently in the current disequilibrated climate. Subsequent analyses focus particularly on these near-thaw sites, where both permafrost occurrence and field testability may be problematic.

CAS were distributed across three land-cover classes. Herbaceous sites are characterized by thick organic mats dominated by *Sphagnum* spp., mosses, tundra grasses, foliose lichens, and earth hummocks, with sparse or absent tree cover; this class represents the most likely ecosystem-protected permafrost zones. Forest is the least extensive class, occurring mainly on the south-facing slope of WS01 and locally along an ephemeral stream in WS02. Ground surfaces range from rocky mineral soils to thick vegetation, but this class is distinguished from herbaceous areas because shading and snow accumulation may alter permafrost conditions [65]. Felsenmeer occurs predominantly on slopes and ridgetops in both valleys and is defined by large, irregular frost-shattered clasts over black shales, laminated siltstones, and weathered dolostone/limestone (Yukon Geological Survey, 2022; [49]). These surfaces may have patchy grasses, mosses, or thin soils, and are often associated with negative temperature anomalies and preserved permafrost in otherwise marginal climates [66–68] but are largely impenetrable to human-powered instruments.

3.3 | Ground Thermal Profiling and Data Collection

The primary method of testing at each CAS for this study was ground thermal profiling, previously used by Bonnaventure and Lewkowicz [28], Way and Lewkowicz [69], Léger et al. [33], Holloway and Lewkowicz [70], and Daly et al. [40]. This is a potentially advantageous method in complex environments because it provides multiple temperature measurements throughout the soil column. However, it is important to note that ground thermal profiling is still a discrete method of data collection and is therefore still limited by the number of points, which can be collected in a vast landscape.

Tests were performed over the course of 2 weeks in late August 2023, close to the annual period of maximum ALT. This decreased the likelihood that any encountered cryotic temperatures were the remnants of seasonal freezing and not true permafrost.

The probe used for this study was constructed from a 300-cm length aluminum avalanche probe (see [40]). Thermistors were secured at 25-cm fixed intervals within the probe. Internal mounting of the sensors was necessitated by the rocky nature of a significant portion of the substrate in the study area, to protect the sensors from being damaged or dislodged. However, this also limited the number of sensors, which were able to fit inside the casing, reducing resolution. Ice-point calibration testing (e.g., [71]) determined the sensors to be accurate within ±0.3°C. The thermistors were connected to an ONSET 4-Channel Analog MX1105 logger (±0.3% accuracy) for data collection. Holes were drilled into the probe where the thermistors were fixed to reduce

TABLE 1 | CAS where a successful ground truthing test was performed and near-cryotic or cryotic temperatures were detected at depth (blue). Sites where cryotic temperatures are estimated within 3 m of the surface, via linear regression (yellow). Sites where permafrost was not detected via linear regression within 3 m of the surface (green) and failed tests (red). Where MAGST data are not available (N/A), this represents a site that did not have an MAGST sensor or where the sensor failed. At sites where initial CAS testing failed, there is no available data for minimum temperature at depth (°C) or predicted or observed depth to cryotic isotherm ("N/A").

Site	Landcover	Elevation (m)	MAGST (°C)	Min. temp at depth (°C)	Max test depth (cm)	Predicted or observed depth to cryotic isotherm
WS01 G11	Herbaceous	1070	0.66	0	59	59
WS01 G16	Herbaceous	959	0.97	0.1	63	63
DMP WS02	Herbaceous	1102	0.12	0	80	80
WS02 G25	Herbaceous	1064	−1.5	0.2	61	61
DMP 02	Herbaceous	668	0.98	0	74	74
DMP 56	Herbaceous	1069	1.05	0.1	45	45
GT 8	Herbaceous	1132	N/A	0	165	165
GT 12	Herbaceous	1087	N/A	0.4	68	68
GT 14	Herbaceous	1080	N/A	0.1	184	184
DMPWS01	Herbaceous	980	0.1	1.8	98	113.1
WS01 G04	Forest	1211	2	9.7	49	184.2
WS01 G08	Felsenmeer	1046	−0.3	7.8	61	222.3
WS01 G13	Herbaceous	1039	0.7	8.1	69	250.9
WS01 G14	Forest	1078	0.4	5.8	58	132.5
WS01 G21	Forest	1189	0.5	9.6	52	201.1
WS01 G24	Felsenmeer	1103	−1.6	9.9	50	134.7
WS01 G46	Herbaceous	978	0	0.6	83	97.9
WS02 G03	Felsenmeer	1071	−0.2	10.2	77	259.6
WS02 G04	Herbaceous	1142	0.7	4.3	70	118.1
WS02 G23	Felsenmeer	1173	−1.5	10.5	55	214.7
WS02 G24	Herbaceous	1064	−1.9	5.3	93	188.2
DMP 09	Felsenmeer	1195	−1.4	7.7	70	235.6
DMP 11	Felsenmeer	1212	−3.2	9.5	55	170.6
DMP 12	Forest	1020	1.9	4	69	87
DMP 20	Forest	1024	2.3	9.4	51	235.6
DMP 26	Herbaceous	1141	−2.2	5.4	90	191.7
GT2	Herbaceous	976	N/A	4	74	226.1
GT3	Herbaceous	970	N/A	8.8	71	193.1
GT6	Herbaceous	1010	N/A	3.7	55	68.8
GT7	Herbaceous	1096	N/A	1.7	79	94.5
GT11	Herbaceous	1101	N/A	3.5	61	83.3
DMP 14	Herbaceous	1149	−1.6	8.01	84	393.7
DMP 32	Herbaceous	1042	−4.9	8.5	75	699.5
DMP 57	Felsenmeer	985	N/A	10.9	67	727.2

(Continues)

TABLE 1 | (Continued)

Site	Landcover	Elevation (m)	MAGST (°C)	Min. temp at depth (°C)	Max test depth (cm)	Predicted or observed depth to cryotic isotherm
DMP 15	Felsenmeer	1123	−4.1	10.4	83	1751.4
WS01 G17	Felsenmeer	1274	−1.9	N/A	26	N/A
WS01 G22	Felsenmeer	1270	0.3	N/A	32	N/A
WS02 G08	Felsenmeer	1097	−2.5	N/A	24	N/A
WS02 G13	Forest	1077	1.1	N/A	35	N/A
WS02 G22	Felsenmeer	1115	−0.9	N/A	32	N/A
DMP 04	Felsenmeer	1132	1.76	N/A	26	N/A
DMP 31	Herbaceous	952	3.54	N/A	19	N/A
GT 1	Felsenmeer	975	N/A	N/A	15	N/A
GT 4	Felsenmeer	962	N/A	N/A	39	N/A
GT 5	Herbaceous	945	N/A	N/A	28	N/A
GT 9	Felsenmeer	1080	N/A	N/A	25	N/A
GT 10	Felsenmeer	1092	N/A	N/A	37	N/A
GT 13	Herbaceous	1081	N/A	N/A	18	N/A
GT 15	Felsenmeer	1247	N/A	N/A	35	N/A

Note: Colors indicate where permafrost was detected directly, indirectly, or if the test was failed.

interference by insulation. Gloves were worn during data collection to prevent conductive heat transfer through the aluminum casing.

Upon arrival at each site, a steel frost probe and hammer were used to make a pilot hole for the ground thermal profiling probe. All pilot holes were made within 1 m of the local GTN, on the same surface type (e.g., moss, felsenmeer, and mineral soil). The pilot hole was driven to the maximum possible depth, determined either by the presence of clasts, tree roots, or the frost table. A depth measurement was then taken, excluding any overlying vegetative materials such as moss. There were no cases where a sufficient depth was reached that more than three thermistors could be submerged, except at sites where significant thaw features created open fissures in the ground surface. An additional thermistor was placed 1 cm below the ground cover at each site to take the surface temperature without the influence of direct solar radiation. Submerged thermistors remained in the ground until all channels reached equilibrium (< 0.1°C change per minute, to a maximum of 15 min; [70]). Minimum temperature and maximum depth of each thermistor was recorded. The 0.5°C isotherm was used as a permafrost-positive indicator, due to the impenetrability of the frost table [69, 71].

3.4 | Field Data Processing and Simple Linear Regression

Although the study area is located within the zone of continuous permafrost, cryotic temperatures were not directly detected at the majority of CAS (81.7%). It is probable that this represents a significant number of false negatives, as depth penetration was highly limited by clasts and tree roots. Substantial ALTs likely also contributed, as thaw fissures observed in the landscape in the herbaceous land cover class exceeded 100-cm depth (see Table 1; GT 8 and 14). Additionally, it is well documented that ALT in felsenmeer may reach up to 3–5 m depths due to ventilation, high porosity, and high thermal conductivity [59, 67, 72].

At CAS where cryotic temperatures were not observed in situ, the depth to the 0°C isotherm was estimated using field measurements and a simple linear regression equation (Equation 1) in R Studio (v.4.4.1.). A separate linear regression was fitted between temperature and depth using the thermistor measurements from each CAS, yielding site-specific intercept (β_0) and slope (β_1) values. This linear approximation was used solely to infer whether the 0°C isotherm likely lay shallower or deeper than the maximum probe penetration at that CAS, rather than to derive precise temperature–depth profiles.

The depth of the zero isotherm was calculated as follows:

$$\text{Depth} = 0 - \beta_0 / \beta_1 \quad (1)$$

where β_0 is the intercept (temperature at depth = 0) and β_1 is the slope, or rate of temperature change with depth.

We used this process to estimate the possibility of reaching the 0°C isotherm within the first 3 m of the surface. If the regression did not predict intersection of the cryotic isotherm within 3 m, cryotic conditions were considered undetected within the instrumented depth for the purposes of this study. We selected a 3-m limit to maintain a more conservative assessment, as we

originally anticipated greater vertical resolution from our field data. However, applying a single linear regression model across multiple substrate types assumes homogeneous conductive behavior, which may oversimplify thermal dynamics in heterogeneous materials. Incorporating an assessment of soil texture and geological composition would help address this limitation in future studies.

MAGST was also considered when determining permafrost presence or absence. (Figure 3). Figure 3 summarizes the decision-tree workflow used to evaluate permafrost presence at these CAS. The workflow integrates collected thermal profiling data with climatic data (MAGST) to qualitatively assess confidence in our observations.

MAGST was used as a broad screening variable in the workflow to distinguish sites that were clearly cold enough to support permafrost from those that may have become too warm for confident interpretation. CAS with MAGST $\leq 0.0°C$ were treated as having the highest likelihood of permafrost presence. Sites with MAGST between 0.1 and 0.9°C were treated as a near-thaw sensitivity range, because marginally positive GSTs in ecosystem-protected settings may still overlie lingering permafrost under disequilibrium conditions [35]. Although permafrost has been observed beneath MAGST values warmer than this, the 0.1°C–0.9°C range was selected as a conservative threshold given the limited vertical resolution of the collected data. CAS with MAGST $\geq 1.0°C$ were therefore treated as lower-confidence sites for near-surface permafrost presence.

All sites underwent frost probing first, to determine if it was possible to reach the frost table and obtain a cryotic temperature measurement immediately. Then, the pilot hole made by the frost probe was used to insert the ground thermal profiling probe. Regardless of MAGST, if cryotic temperatures were reached in situ, the site was considered to have permafrost present with high confidence. If MAGST was in the

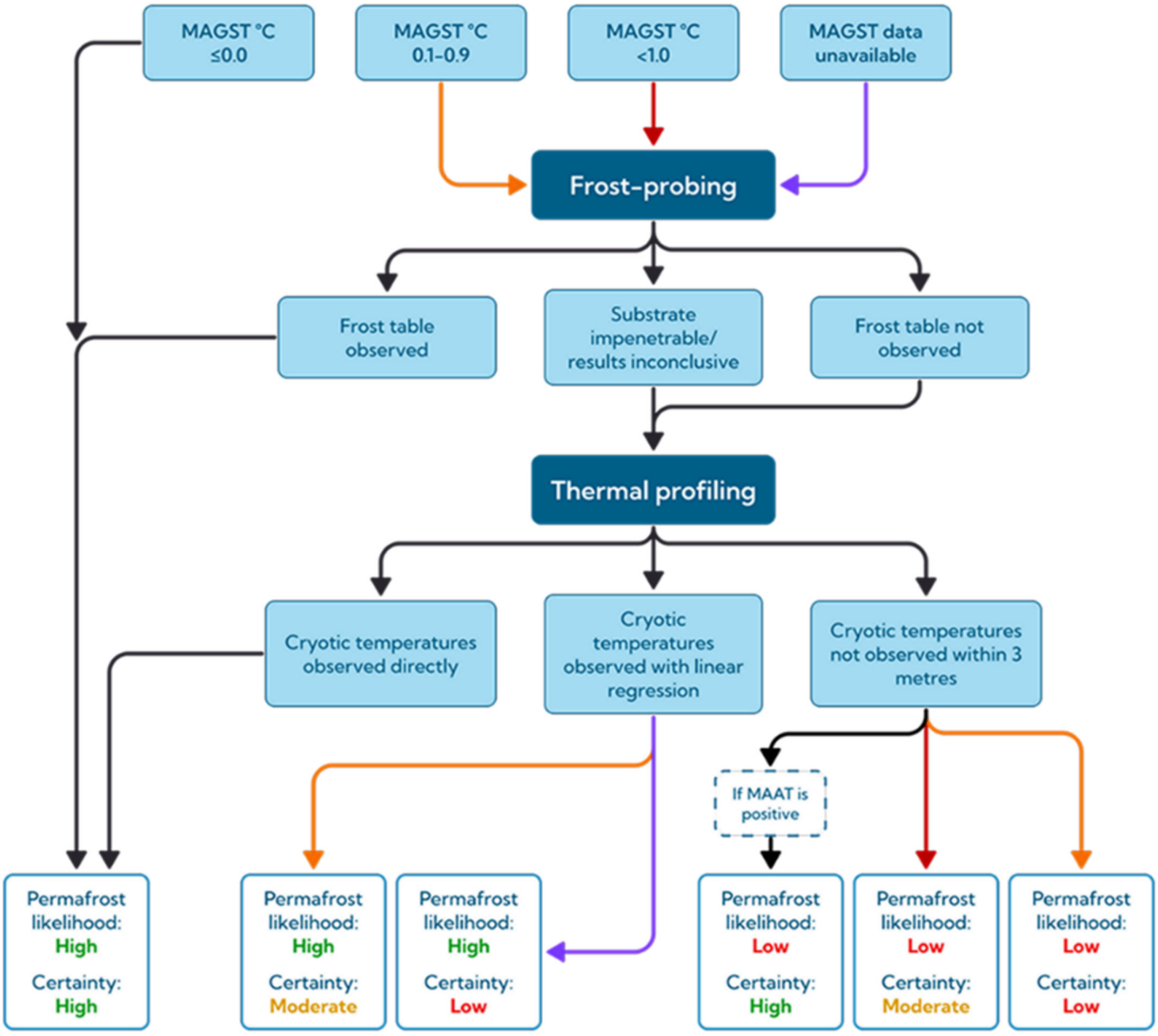

FIGURE 3 | Flowchart demonstrating the decision-making process regarding permafrost presence or absence at CAS. [Colour figure can be viewed at wileyonlinelibrary.com]

near-thaw sensitivity range (0.1°C–0.9°C) but cryotic temperatures predicted via linear regression within 3 m of the surface, our certainty of a permafrost positive site was high with moderate confidence. Confidence is reduced because linear regression is an indirect, statistical confirmation of permafrost, rather than a direct observation of cryotic temperatures. If MAGST ≥ 1.0°C, and cryotic temperatures were not reached in situ, confidence in linear regression estimations was also reduced. However, if MAGST ≥ 1.0°C and cryotic temperatures were not observed within 3 m via linear regression, this represented a greater confidence estimation of permafrost absence.

3.5 | Probability Surface Generation (P_{TEST} Model)

Observations of test failure and test success at all CAS were used to generate a probability surface of permafrost testability (P_{TEST}), for application to the larger subrange of the Ogilvie Mountains beyond the mountain valley study area. At this stage, permafrost presence or absence was not considered, only the binary metric of "test success" or "test failure." We defined test success and test failure based on maximum depth of the probe. CAS where the probe could not penetrate to a depth of 45 cm or greater were considered to represent failed tests. This threshold was not selected to represent typical ALT in the study area, nor does it imply that permafrost is necessarily expected at this depth across the study area. Instead, this metric was chosen because it represents the shallowest depth at which cryotic temperatures were observed in the field. It is intended to function as a conservative and internally consistent minimum depth for defining "successful" testability in this study. Given the limited duration of the field season and noted accessibility issues of the study area, the sampling prioritized CAS within the near-thaw sensitivity range (MAGST = 0.1°C–0.9°C). These conditions occur due to ecosystem-protected permafrost, which in our study area was in herbaceous class sites found only at lower elevations. This resulted in a biased data set. To address this bias, we used random stratification to select an additional 25 sites from the preexisting network of GTN loggers already known to be untestable due to extremely hard, clast-dense substrates lacking any form of soil development. These sites have been visited by researchers in previous years to install GTNs and air temperature sensors, and field conditions there are well documented. At these sites, the environment is defined by felsenmeer with no soil development. Although the probe could be placed between the clasts, this would only produce an air temperature measurement, rather than a ground temperature measurement. Penetration beyond 45 cm is also highly improbable. The sites were chosen from a range of elevations from both WS01 and WS02, but trend toward higher elevations due to the inherent patterns of geology and soil development in the region.

To create the P_{TEST} model, a 2-m digital elevation model (DEM) of the study area was derived from optical imagery by the Polar Geospatial Center at the University of Minnesota [73]. Potentially relevant environmental variables (slope, aspect, topographic position index [TPI], and elevation) were extracted from the DEM using ArcPro v. 3.3.0 and the Jenness TPI extension (v.1.3; [74]).

Prior to modeling, the DEM-derived environmental variables were examined for multicollinearity using Pearson's correlation and variance inflation factors (VIF) analysis in RStudio v.4.4.1. No strong correlations between variables were detected. Logistic regression, implemented through the caret (Classification and Regression Training) package [75] was used to evaluate the influence of all candidate variables on the probability of conducting a successful test. Of these, only elevation was statistically significant (Table 2), and was therefore defined as the sole predictor variable for subsequent model development. Given the modest sample size and our focusing on characterizing overall testability patterns, we opted to use this simpler model rather than constructing a highly parameterized model. We recognize that more complex nonlinear relationships may exist but could not robustly be estimated here.

TABLE 2 | The coefficients table associated with the general linear model.

	Estimate	Standard error	z	Pr(>|z|)
Intercept	23.5441905	9.3274613	2.524	0.0116
Land cover	−0.1031750	0.5790599	−0.178	0.8586
Aspect	−0.0001016	0.0042850	−0.024	0.9811
Slope	−0.0054994	0.0387279	−0.142	0.8871
TPI	1.2661861	1.1235530	1.127	0.2598
Elevation	−0.0201476	0.0078750	−2.558	**0.0105**

Field data were then randomly divided into a training set (comprising 70% of the data) and a testing set (comprising 30%). A logistic regression model was applied to predict the probability of a successful test, producing values between 0.0 and 1.0 using Equation (2), where y is the linear predictor derived from the fitted intercept and coefficient for elevation (e.g., [58]).

$$P_{TEST} = 1 / (1 + \exp(-y)) \quad (2)$$

where y is defined by Equation (3).

$$y = \beta_0 + \beta_1 (\text{Elevation}) \quad (3)$$

Using the point predictions from the model, a continuous probability surface was generated with the Raster Calculator tool in ArcGIS Pro (Figure 4).

3.6 | Model Comparison

The P_{TEST} model was then compared with the results of two other local models of permafrost distribution, Bonnaventure et al. [58] and Garibaldi et al. [53]. The goal of this comparison was to identify zones where warm, "near-thaw" permafrost (MAGST = 0.1°C–0.9°C), which is more immediately vulnerable to thaw intersects with zones of low testability. These areas represent the greatest uncertainty, where it is unclear how soon permafrost will thaw under current climate conditions and it is also unclear if those conditions can be verified. The P_{TEST} model was grouped into four probability classes (0–0.25, 0.25–0.5, 0.5–0.75, and 0.75–1.0) for this comparison.

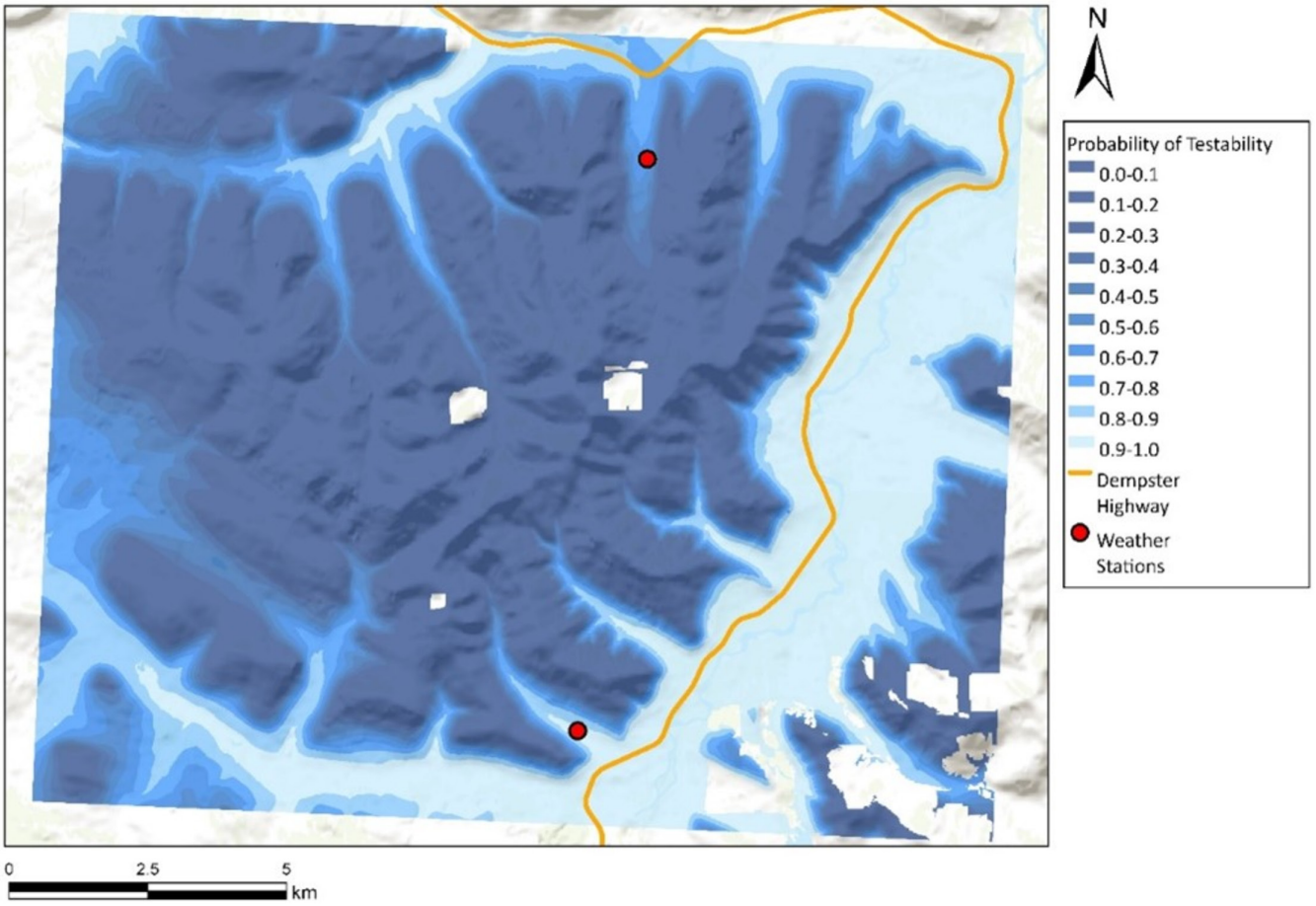

FIGURE 4 | Probability of conducting a successful permafrost test in an expanded zone beyond the original study areas. Areas with no modeled results represent gaps in the DEM. The P_{TEST} model layer is set at 50% transparency for clarity. *Basemap Imagery: Maxar Technologies, Esri, Earthstar Geographics*. [Colour figure can be viewed at wileyonlinelibrary.com]

The Bonnaventure et al. [58] model is a moderate- to high-resolution (30 × 30 m) permafrost probability model covering much of northern British Columbia and Yukon, including the study area near the northern limit of its extent. It was developed by combining several empirical-statistical models and broadly validated using discrete ground-truthing sites and long-term borehole data, with Dawson City, YT, representing the nearest validation area to this study. Model outputs are expressed as permafrost probability and can be grouped into continuity classes such as sporadic, extensive-discontinuous, and continuous. The extensive-discontinuous class was treated as a lower-certainty transition category for comparison with P_{TEST}; no part of the study area was classified as sporadic by this model.

The Garibaldi et al. [53] model is a process-based TTOP model derived from several years of in situ climatological data collected from the ground-temperature monitoring network in WS01 and WS02. Rather than probability, it outputs predicted subsurface temperatures under equilibrium conditions. For comparison with P_{TEST}, TTOP values were interpreted primarily relative to the equilibrium threshold of 0°C, with TTOP $\leq$ 0°C indicating thermally favorable conditions for permafrost in the model framework and TTOP > 0°C indicating thermally unfavorable conditions.

In addition, we examined a near-thaw positive TTOP range as a sensitivity zone, rather than as a formal permafrost class, in order to highlight terrain where equilibrium-based TTOP may underrepresent lingering or ecosystem-buffered permafrost under disequilibrium conditions, and where field validation may also be especially difficult. This rationale is consistent with recent work showing that equilibrium TTOP approaches can underpredict permafrost in disequilibrium settings unless calibrated against field observations [76]. Because the interpretation of this near-thaw range depends on threshold choice, we also repeated the analysis using a broader sensitivity threshold defined by TTOP = 0.0°C–2.0°C.

To quantitatively compare model performance at the CAS locations, we constructed confusion matrices for the following three models: (i) the Bonnaventure et al. [58] permafrost probability model, (ii) the Garibaldi et al. [53] TTOP model, and (iii) the P_{TEST} testability model. For each model, permafrost presence/absence (or testable/not testable in the case of P_{TEST}) was defined using the same binary thresholds as stated. From these confusion matrices, standard classification metrics were calculated, including overall accuracy, sensitivity (true positive rate), specificity (true negative rate), precision, and F1 score. Metrics were computed only at CAS where field observations allowed permafrost presence or absence to be confirmed to ensure a consistent basis for comparison.

4 | Results

4.1 | Field Results

A total of 49 CAS were sampled throughout the 2023 field season (Figure 5). Of these, 36 were considered successful, meaning that the probe was able to reach the minimum benchmark of 45-cm B.D.

4.2 | Permafrost Detected Directly

Of the 36 successful tests, only nine CAS (18.3%) produced cryotic temperatures in situ. Three of these CAS were thaw features in the landscape, where thaw disruption created fissure-like features in the valley bottoms and allowed the probe to reach a greater than normal depth. The average depth of cryotic materials was 89-cm B.D., with a minimum of 45 cm and a maximum of 184 cm (Table 1). Excluding these fissures, the average active layer depth was 63 cm. Where data were available, all sites except one had a positive MAGST. Overall, the sites were constrained to the lower elevations of the valleys, ranging from 668- to 1149-m elevation (average 1041 m). All of these sites were located within the herbaceous land cover class.

4.3 | Permafrost Detected via Linear Regression

Of the successful CAS tests, 22 (61.0%) did not produce cryotic temperatures in situ but are predicted to have cryotic materials

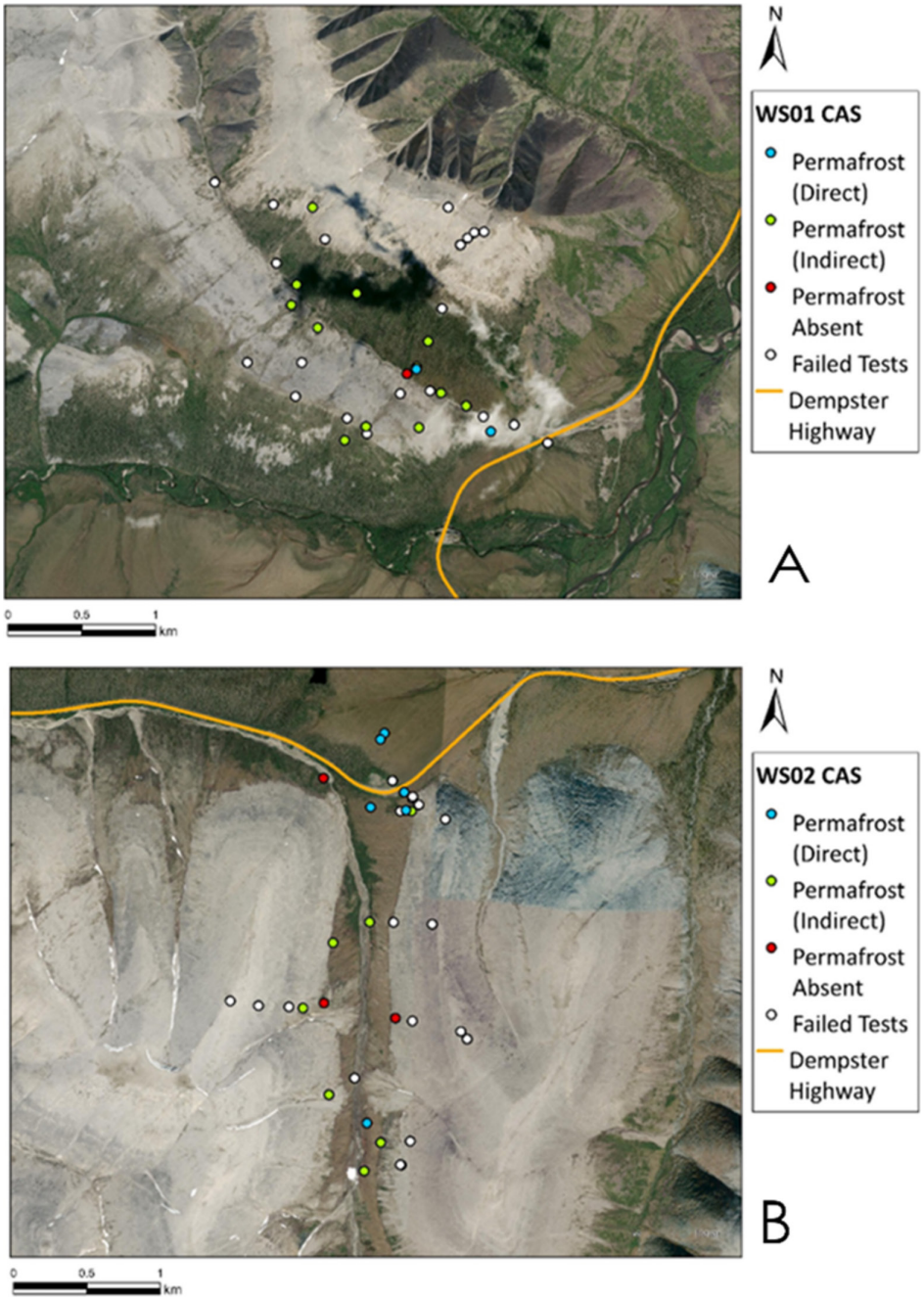

FIGURE 5 | Distribution and results of ground truthing tests in WS01 (A) and WS02 (B). *Basemap Imagery: Maxar Technologies, Esri, Earthstar Geographics*. [Colour figure can be viewed at wileyonlinelibrary.com]

within 3 m of the surface (Table 1). Of these tests, in the herbaceous land cover class, the average ALT prediction is 148-cm B.D., ranging from 68 to 250 cm. In the felsenmeer land cover class, the average ALT prediction is 206 cm, ranging from 134 to 259 cm. In the forest land cover class, the average ALT prediction is 87–235 cm.

4.4 | No Permafrost Detected Within 3 m of Surface

Sites were declared as operationally "permafrost absent" for near-surface permafrost when the linear regression equation did not predict crossing the 0°C isotherm within the first 3 m of the surface (Table 1). Four of the successful tests produced results that suggest permafrost is not present below the subsurface within 3 m.

4.5 | Failed Tests

Of the 49 total CAS sampled, 14 tests were considered to have failed because of not reaching the 45-cm B.D. benchmark (Table 1). The average depth achieved at failed sites was 27 cm. Sites ranged in elevation from 945 to 1247 m, with an average elevation of 1092 m. Most failed tests (71.4%) were at an elevation greater than 1000 m. Test failures occurred because of the presence of impenetrable substrates, clasts in the subsurface, or tree roots.

4.6 | Testability Model (P_{TEST} Model)

Several environmental variables were considered to inform the P_{TEST} model. However, only elevation emerged as statistically significant (Table 2).

The P_{TEST} model was overlaid across the subrange and reclassified into probability zones, ranging from 0% to 100% likelihood of a successful test (Figure 4). The total extent of the selected area is approximately 247 km^2. The probability of P_{TEST} success increases toward areas of lower elevation.

Most of the landscape falls either into the extremely low or extremely high P_{TEST} probabilities. The majority of WS01 (51.3%) falls within the range of low testability (0%–25% likelihood), and 26.6% falls within the range of high testability (75%–100%) (Figure 6). The majority of WS02 (68.7%) falls within the zone of low testability, and only 6.4% falls within zones of high testability (Figure 6). It should be noted that, on average, the elevation of WS02 is approximately 100 m higher than that of WS01.

4.7 | Model Comparisons

4.7.1 | Comparison With Bonnaventure et al.

The Bonnaventure et al. [58] model predicts permafrost probability across the study area, with values ranging from 40% to 100%. For comparison with this study, we grouped probabilities into continuity classes: 0%–39% as sporadic, 40%–70% as extensive-discontinuous ("marginal"), and 71%–100% as continuous. Across the subrange, 74.5% of the land area is classified as extensive-discontinuous permafrost and 24.6% as continuous.

In WS01, the lowest permafrost probabilities (40%–50%) occur on the forested south-facing slope, but field tests there were inconclusive because dense subsurface roots prevented sufficient probe penetration. When compared with P_{TEST}, zones of low testability (0%–25%) overlap strongly with high modeled permafrost probabilities: the mean Bonnaventure et al. probability in this class is 80.0%, compared with 69.2% in the highest-testability class (75%–100%). The single permafrost-absent CAS in WS01 also falls within a relatively high modeled permafrost probability zone (80%–90%) on the valley bottom (Figure 7A).

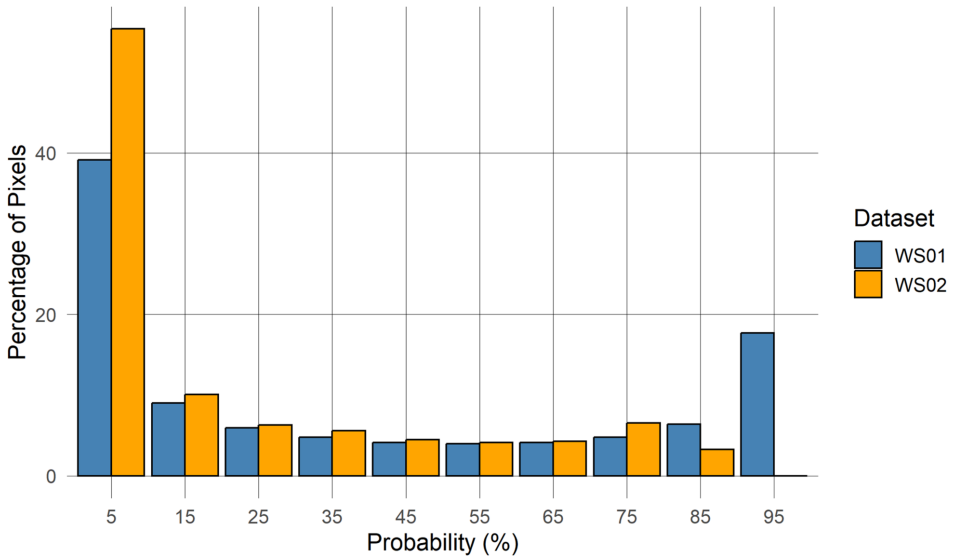

FIGURE 6 | Distribution of probabilities of permafrost test success in WS01 and WS02 against percentage of total area in the subrange. [Colour figure can be viewed at wileyonlinelibrary.com]

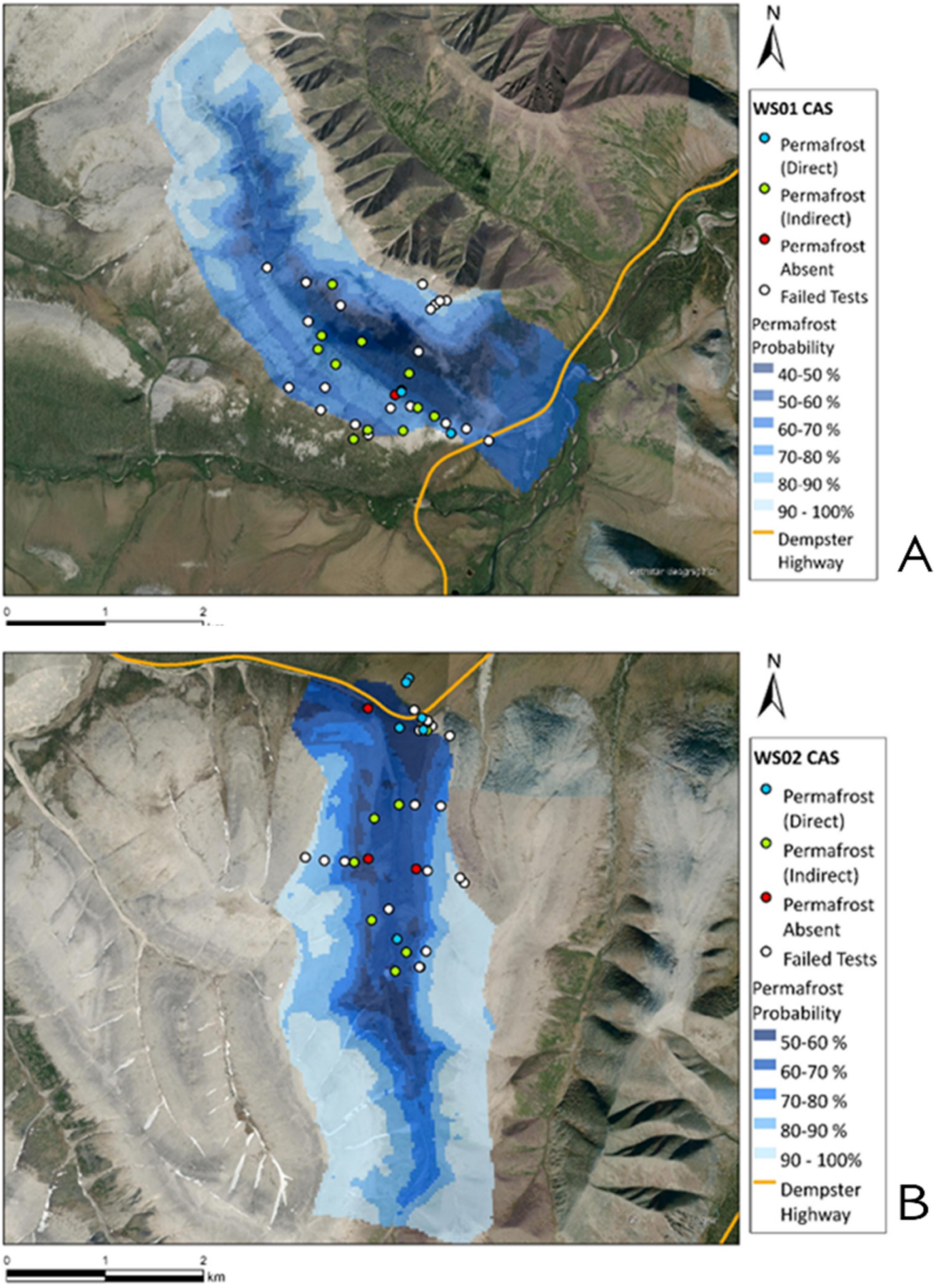

FIGURE 7 | CAS testing against the Bonnaventure et al. [58] probability model in WS01 (A) and WS02 (B), set to 50% transparency for clarity. *Basemap Imagery: Maxar Technologies, Esri, Earthstar Geographics.* [Colour figure can be viewed at wileyonlinelibrary.com]

TABLE 3 | A comparison of permafrost probability values modeled by Bonnaventure et al. [58] and P_{TEST} values in WS01 and WS02.

P_{TEST}	Site	Permafrost probability (min.) (%)	Permafrost probability (max.) (%)	Permafrost probability (mean) (%)
Low: 0%–25%	WS01	46.1	98.4	80.0
	WS02	58.8	98.5	88.1
Moderate: 25%–50%	WS01	40.7	73.0	57.7
	WS02	50.8	75.4	62.3
High-moderate: 50%–75%	WS01	42.8	74.7	60.0
	WS02	50.9	74.1	62.2
High: 75%–100%	WS01	46.6	78.7	62.9
	WS02	51.4	72.3	59.6

A similar pattern is evident in WS02. The lowest modeled permafrost probabilities (50%–60%) occur in the valley bottom (Figure 7B). One CAS in this class was classified as permafrost absent using linear regression, yet cryotic temperatures were detected in situ only 378 m away in the same probability zone. Of the three permafrost-absent CAS in WS02, two occur within the 60%–70% probability class and one within the 40%–50% class. As in WS01, mean permafrost probability is highest in the low-testability class and lowest in the high-testability class (Table 3), averaging 88.1% in the 0%–25% P_{TEST} class and 59.6% in the 75%–100% class.

When interpreting the comparison between P_{TEST} and the Bonnaventure et al. [58] permafrost-probability model, it is important to recognize that the two products operate at different native resolutions. Some of the apparent small-scale disagreement between the two products is thus expected from the scale mismatch and associated smoothing, rather than indicating a fundamental inconsistency in permafrost conditions. This overlay is intended to be interpreted heuristically to identify broad zones where testability and modeled permafrost uncertainty co-occur, rather than a strict pixel-by-pixel accuracy assessment.

4.7.2 | Comparison With Garibaldi et al.

The Garibaldi et al. [53] TTOP model is limited spatially to WS01 and WS02, so the comparison presented here is restricted to those valleys. For this comparison, TTOP ≤ 0°C was interpreted as indicating thermally favorable equilibrium conditions for permafrost, whereas TTOP > 0°C was interpreted as thermally unfavorable. We also examined a near-thaw positive TTOP range (0.1°C–0.9°C) as an operational sensitivity zone to identify terrain where equilibrium-based TTOP may underrepresent lingering permafrost under disequilibrium conditions. Under this interpretation, the Garibaldi et al. model predicts that 82.5% of WS01 has TTOP ≤ 0°C, while 8.6% falls within the near-thaw sensitivity range and 8.7% has TTOP ≥ 1.0°C (Figure 8A). In WS02, 99.2% of the valley has TTOP ≤ 0°C, 0.7% falls within the near-thaw range, and only 0.002% has TTOP > 1°C (Figure 8B).

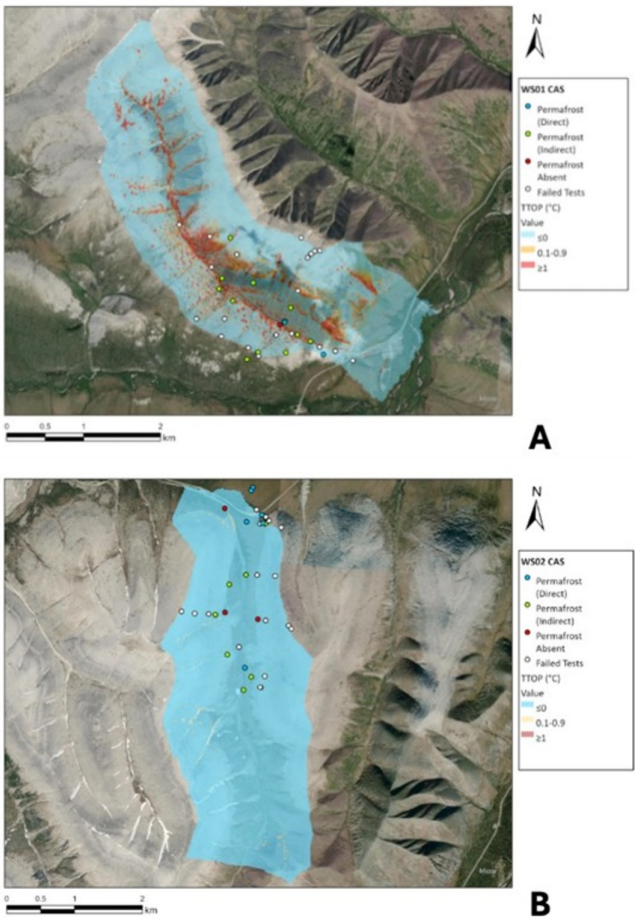

FIGURE 8 | The TTOP model by Garibaldi et al. [53] compared against the results of CAS testing in WS01 (A) and WS02 (B). The model is set to 50% transparency for clarity purposes. *Basemap Imagery: Maxar Technologies, Esri, Earthstar Geographics*. [Colour figure can be viewed at wileyonlinelibrary.com]

Comparison with P_{TEST} shows that, in WS01, colder TTOP values are associated with both low (0%–25%) and high (75%–100%) testability, whereas the warmest TTOP conditions (mean ≈ −0.1°C) occur within the moderate P_{TEST} classes (25%–75%) (Table 4 and Figure 8). Mean TTOP values in the low- and

high-testability classes were −2.3°C and −1.3°C, respectively. In WS02, the relationship is less consistent, with colder TTOP values across all testability classes and weaker separation among them (Table 4). The warmest average TTOP occurs in the 75%–100% class (−1.8°C), while the coldest mean TTOP falls within the 50%–75% class.

We also conducted a sensitivity analysis in which the upper limit of the near-thaw sensitivity range was increased to 2.0°C. Under this broader threshold, WS01 was classified as 81.1% permafrost, 16.5% uncertain permafrost, and 2.3% permafrost absent. This result reinforces that the near-thaw sensitivity category is an operational class intended to highlight potentially vulnerable or misclassified terrain; although the proportions of area in each class shift with threshold choice, the broader spatial patterns remain qualitatively consistent.

TABLE 4 | A comparison of TTOP (°C) values modeled by Garibaldi et al. [53] with categories of P_{TEST} in WS01 and WS02.

P_{TEST}	Site	TTOP min. (°C)	TTOP max. (°C)	TTOP mean (°C)
Low: 0%–25%	WS01	−5.3	3.7	−2.3
	WS02	−5.5	0.52	−2.1
Moderate: 25%–50%	WS01	−5.8	3.3	−0.1
	WS02	−4.8	0.58	−1.9
High-moderate: 50%–75%	WS01	−5.7	3.3	−0.1
	WS02	−5.9	0.75	−2.2
High: 75%–100%	WS01	−9.4	3.1	−1.3
	WS02	−4.9	1.0	−1.8

TABLE 5 | Sensitivity analysis of overlap between P_{TEST} probability classes and near-thaw TTOP terrain from the Garibaldi et al. [53] model in WS01 and WS02. Values show the percentage of each valley occupied by overlapping classes under the original threshold (0.1°C–0.9°C) and a broader sensitivity threshold ("SA 2.0+"), allowing assessment of whether the relationship between reduced testability and thermally sensitive terrain is robust to threshold choice.

	WS01		WS02	
P_{TEST}	0.1–0.9	SA 2.0+	0.1–0.9	SA 2.0+
0–0.25	8.38	7.94	60.10	66.10
0.25–0.5	35.65	32.18	20.64	17.41
0.5–0.75	43.61	46.01	19.26	16.49
0.75–1.00	12.36	13.88	0	0

To further evaluate the relationship between P_{TEST} and the Garibaldi et al. [53] TTOP model, we examined how the overlap between P_{TEST} classes and near-thaw TTOP terrain changed under the original and broadened sensitivity thresholds (Table 5). Under the original definition, the greatest overlap generally occurred within the moderate P_{TEST} classes (0.25–0.75), whereas the highest-testability class showed less overlap. In WS01, the 0.5–0.75 P_{TEST} class had the strongest overlap with the 0.1°C–0.9°C near-thaw TTOP zone; in WS02, overlap was greatest in the 0–0.25 and 0.25–0.5 classes. Repeating the analysis with the broader threshold ("SA 2.0+") produced broadly similar class-wise patterns, indicating that the observed relationship between reduced testability and thermally sensitive terrain is not an artifact of the original threshold definition.

At the CAS scale, these qualitative patterns are reflected in the quantitative performance metrics (Table 6). The Bonnaventure et al. [58] probability model achieves high overall accuracy and very high sensitivity but essentially zero specificity, indicating a strong tendency to predict permafrost presence at nearly all sites. The TTOP model shows more balanced behavior, with moderate sensitivity and somewhat improved specificity, but still generally overpredicts permafrost. In contrast, the P_{TEST} model exhibits the most balanced trade-off between detecting testable and nontestable locations, with comparable sensitivity and specificity and the highest F1 score among the three models. These metrics provide a more rigorous basis for the model comparison and support the use of P_{TEST} as a tool for identifying where field validation is feasible.

5 | Discussion

This study encountered substantial challenges in data collection, due to greater-than-anticipated difficulties with substrate penetrability and noted limitations of site accessibility. Although these constraints were considered during the project's conceptualization, they proved to be more severe than anticipated. However, these difficulties exemplify the core of our research questions and highlight that the Ogilvie Mountains (and similar heterogeneous periglacial terrains) are still the subject of a significant knowledge gap with regards to testability.

TABLE 6 | Summary of model performance metrics at CAS locations for the Bonnaventure et al. [58] probability model, the Garibaldi et al. [53] TTOP model, and the P_{TEST} testability model.

Model	Accuracy	Sensitivity	Specificity	Precision	F1
Bonnaventure et al. [58]	0.824	0.966	0.000	0.848	0.903
Garibaldi et al. [53] TTOP	0.643	0.708	0.250	0.850	0.773
P_{TEST} testability	0.685	0.765	0.615	0.634	0.693

5.1 | Potential for False Negatives or False Positives in CAS Testing

It is unlikely that any of the cryotic temperatures encountered in situ were false positives (i.e., the remnants of seasonal freezing) due to the timing of the fieldwork and the observed ALT across all sampled CAS. Although false positives may have occurred in instances where linear regression was used to estimate depth to the cryotic isotherm, it is more likely that the estimated depth is erroneous, rather than the actual presence of permafrost—especially at sites with subzero MAGST values.

False negatives are more likely. Of the 36 successful tests performed, only 4 were determined not to have permafrost present via linear regression. Although these areas may represent zones of near-surface permafrost loss, the limitations of the instrument and lacking baseline data on ground thermal state make it difficult to comment on that with any confidence. Sites determined not to have permafrost in this context were given this designation because linear regression did not predict cryotic temperatures within the first 3 m of the surface, but it is possible for ALT to exceed 3 m in some environments [59]. In the field, we observed and documented instances of thaw disturbance creating fissures > 100 cm deep, which exceeds the maximum depth that the probe was capable of penetrating to at the majority of CAS Observations of deep active layer thickening are consistent with observations of others around the Dempster Highway (e.g., [41, 77]). However, it is unclear if the disturbances witnessed represent actual near-surface permafrost loss, or if they will refreeze or develop taliks.

5.2 | Influences on CAS Field Results

5.2.1 | Felsenmeer

Most logistical challenges associated with testing for permafrost in WS01 and WS02 are associated with the felsenmeer land cover type, which covers the majority of the subrange. The felsenmeer-covered valley walls are extremely steep (up to 69°), and many of the clasts are unstable, which poses a considerable safety risk to researchers attempting to climb them. Where the valley walls are not steep (such as on the ridgetops and in proximity to the valley bottoms), the terrain may still be unstable because of the unfixed clasts. Not only are these sites difficult to reach, but they frequently yield minimal results when tested.

Felsenmeer sites made up the majority of untestable CAS due to their shallow or nonexistent soil profiles. Where soil was present, the probe was generally unable to reach depths where a significant number of sensors were below the surface due to the dense concentrations of clasts. Although it was sometimes possible to maneuver the probe between the clasts, this rarely yielded meaningful results. At sites where no soil profile was present, probing between the clasts would have only yielded an air temperature measurement. However, these sites likely have continuous permafrost coverage.

Felsenmeer sites in both WS01 and WS02 are cold on average, with MAGSTs at sampled CAS averaging −1.3°C. However, we were unable to reach cryotic temperatures in situ at any of them, likely due to much deeper active layers. The felsenmeer land cover type (and similar rocky, low-moisture environments) is well understood to have a fast response time to ambient air temperatures. This is due to high thermal conductivities and frequently, a lack of ground ice, meaning that large amounts of thaw can occur in a relatively short period of time [59]. This may be up to 5 m [72], and if this were the case, the active layer would have exceeded the full length of the ground thermal profiling probe. However, there were no instances in felsenmeer where we were able to penetrate up to even 1 m.

In these environments, permafrost is categorized as dry due to the lack of ground or pore ice, and cryotic materials are largely restricted to the clasts. The result is that permafrost thaw is unlikely to produce surface features like retrogressive thaw slumps and active layer detachments. This lack of ice and organic carbon also means that thaw in dry permafrost environments is less likely to result in environmental disturbances [78]. Therefore, although uncertainty associated with distribution and thermal state in dry permafrost environments is not ideal, it is less detrimental than uncertainty associated with ice- or carbon-rich permafrost environments.

There are no rock glaciers present within the study area. However, probing the felsenmeer sites could be considered a close analog to probing a rock glacier. A growing number of studies in the European Alps have documented internal structures or ice cores in rock glaciers using boreholes (e.g., [31, 79]) and geophysical surveys (e.g., [80]). However, many investigations still rely on indirect methods such as electrical resistivity tomography (e.g., [81]) and ground penetrating radar (e.g., [82]).

5.2.2 | Impacts on Model Results

Five DEM-derived variables were considered as potential drivers for the likelihood of P_{TEST} success: land cover, TPI, aspect, slope, and elevation. However, only elevation was identified as a significant predictor by the logistic regression analysis, showing a small but statistically significant negative impact on the dependent variable P_{TEST}. This is likely due to the relationship between elevation and soil development in the study area. However, we do not interpret this to mean that elevation alone controls testability. Rather, elevation is likely acting as a proxy for a suite of co-varying factors, including the distribution of blocky felsenmeer versus finer-grained soils, the degree of soil and organic layer development, and vegetation cover. Micro-topographic variability (e.g., slope breaks, aspect, and concavity) strongly influences where fine particles accumulate, where soil moisture is retained, and where dense clast layers are exposed at the surface, all of which directly affect both the ease of probe insertion and the stability of the ground surface during fieldwork.

The contrast between WS01 and WS02—where WS02 has a higher proportion of herbaceous cover but a lower proportion of high-testability area—likely reflects such valley-specific differences in substrate and micro-topographic configuration, rather than elevation alone. In this sense, the elevation term in P_{TEST}

should be viewed as a proxy for these linked processes at the scale and sample size of our dataset, with the understanding that more detailed terrain, snow, and substrate information would be required to explicitly resolve their individual contributions.

Aspect was initially considered a potential driver of testability due to its influence on surface energy balance, which affects vegetation species and coverage, moisture content, permafrost distribution, frequency of freeze–thaw cycles, and soil texture [83]. However, the logistic regression analysis revealed it to be the most statistically insignificant variable, with a Pr(>|z|) value of 0.98. In WS01, the influence of aspect manifests visibly as a forest-covered south-facing slope and a felsenmeer-covered north-facing slope. The next nearest valley, north of WS01, lacks this difference and visible treeline. In WS02, aspect seems to have a weaker visible influence. Neither side of this valley is treed and soil distribution on the slopes is uniformly lacking on both sides. Ultimately, it is likely that aspect was statistically insignificant because (1) aspect did not have a strong influence on soil development in WS02 and (2) most failed tests occurred because of impenetrable substrate and clast presence, not tree roots, negating the impact of the forest land cover class.

Following aspect, slope is the next most statistically insignificant variable (Pr(>|z|) = 0.88). It was initially considered a potential predictor due to its strong influence on drainage and its potential association with the felsenmeer land cover type. CAS were slightly biased toward sites with lower slope angles due to terrain hazards and the instability at higher elevations on felsenmeer slopes, where clasts were loose and lacked soil. This bias may explain the variable's insignificance.

Land cover is only marginally less significant than slope (Pr(>|z|) = 0.85), which was surprising given it was initially hypothesized to be the determining factor for P_{TEST} success. From aerial or site-level observations, it seemed intuitive that rocky areas would be less testable than herbaceous areas. Felsenmeer seemed to be totally lacking in testability, while the herbaceous class was anticipated to be uniformly successful. However, upon testing, it became clearer that the testability of the area is as heterogeneous as its permafrost distribution. Although it was generally true that felsenmeer restricted testability, there were rare cases where soil development was deeper than anticipated, and it was possible to penetrate to greater depths than assumed when observing the surface. Inversely, some herbaceous sites proximal to the valley walls concealed felsenmeer beneath vegetation, resulting in limited test success where we assumed that it would be possible to reach significant depths.

TPI also did not approach statistical significance (Pr(>|z|) = 0.25). TPI was originally selected because it seemed likely that convex sites such as ridgetops would have significantly lower testability than concave locations, where water pooling and deeper snow cover would be more likely to occur.

Although this model did not find any of the DEM-derived variables to be relevant, sans elevation, this may not be the case in other environments. In the case of the Ogilvie Mountains, we believe that elevation was the ultimate predictor of P_{TEST} due to its relationship with wind-scouring and soil development. However, in another research environment, such as a High Arctic environment with polar bedrock landcover (see [59]), P_{TEST} would likely still be low at low elevation. This is because the physical mechanism determining testability is substrate hardness.

Overall, it is unlikely that elevation is the sole predictor of test success, but the spatiotemporal resolution of the sampled sites may be too low to capture the full complexity of the actual variables. Ultimately, all variables other than elevation were excluded from the probability model. However, there are drawbacks. Because WS01 is situated approximately 100 m lower than WS02, the model predicts a broader range of testability probabilities in WS01 compared to WS02. In WS01, probabilities range from 0% to 100%, whereas in WS02, probabilities range from 0% to 90%. This occurs despite WS02 having more coverage of the herbaceous land cover class, which is the most successful land cover class for P_{TEST}.

5.2.3 | Surficial Temperature Measurements as Permafrost Indicators

It is well understood that permafrost is defined by its cryotic isotherm [84], and many assessments of permafrost conditions assess GSTs as potential indicators of permafrost presence (e.g., [85–89]). Generally, GST is considered to be a reliable indicator of permafrost presence [88] and a good indicator of overall climate, as it integrates the influence of atmospheric conditions with ground conditions (e.g., snow cover, vegetation, and microrelief) [90]. This is the general principle behind some remote sensing-based permafrost evaluations (e.g., [91, 92]), and collecting data from remote sensing instruments is a much faster and cost-effective way to obtain spatially dense temperature data across landscapes [91].

However, the effectiveness of using surficial measurements to indicate conditions deeper in the soil profile has been challenged [93, 65]. Using surficial measurements to indicate permafrost presence is especially problematic in areas like the north-central Yukon, where there is frequently a disconnect between the air and GST, resulting in significant surface offsets [94]. This effect was observed several times in our research. All CAS, which produced an in situ cryotic temperature measurement, were in the herbaceous land cover class, which features thermally insulative vegetation that produces surface offsets/ecosystem-protected permafrost. All but one of these sites had a positive MAGST (0.1°C–1.0°C). Furthermore, eight of the 22 sites with permafrost predicted by linear regression also had positive MAGSTs, with one as warm as 2.0°C.

5.3 | Errors, Limitations, and Uncertainties

5.3.1 | Ground Thermal Profiling Instrument

This study represents a prototype attempt to assess the study area and is not intended to be viewed as an optimized approach to ground thermal profiling. The primary objective of the research was to assess the viability of testing itself in a challenging environment, with the understanding that future iterations of the study should refine the instrumentation and methods based

on these initial findings. The following section will discuss the challenges we encountered in the field and their impact on the final results.

We employed a method of ground thermal profiling wherein the individual thermistors were mounted at fixed intervals within the probe's casing, to prevent displacement or damage from clasts during insertion into the substrate. Internally mounting the thermistors in this fashion limited the number of possible sensors inside the casing, due to the thickness of the wires. However, this configuration was still seen as preferable to external mounting, due to the high likelihood of damage by clasts. Although increasing the casing's diameter would allow for it to accommodate more sensors, it would also reduce the probe's ability to effectively navigate between clasts.

The 3-m probe length was selected to balance the objective of achieving sufficient penetration depth within the logistical constraints of deployment in remote, high-relief terrain. Although it is true that we expected to encounter felsenmeer, which may have active layers up to 5 m deep [59, 72], we assessed that it was highly improbable we would be capable of achieving that depth due to the blocky nature of the substrate. Because the probe had to be transported over long distances and steep slopes, often across rocky and unstable surfaces, increasing the probe length would have increased the physical burden on field personnel. This would have further limited site accessibility and sampling efficiency. Therefore, the 3-m length represented a pragmatic compromise between maximizing potential sampling depth and maintaining operational feasibility and safety in the challenging terrain.

During the design phase of the field campaign, it was anticipated that at the very least, most CAS in the herbaceous class would be able to be penetrated up to the full length of the probe (3 m). However, in the field, we encountered buried felsenmeer at surprisingly shallow depths beneath the thick organic soils and moss cover of the herbaceous and forest land cover sites. This significantly reduced the number of thermistors that were submerged in the subsurface at any given time. We recognize that our data resolution would be significantly improved by reducing the vertical spacing between the sensors (e.g., [33]). Ultimately, the larger vertical spacing of our thermistors is likely to have caused our sensors to miss critical thermal inflection points near the frost table. Additionally, the lower number of sensors does not sufficiently fully capture the variability of temperature change due to the lag effect of heat moving through the soil column. In some cases, we noted a minor temperature increase in the at shallow depths below the surface, which represented this.

5.3.1.1 | Linear Regression of CAS Data. A further limitation arises from the use of simple linear temperature–depth extrapolation to estimate the 0°C isotherm at sites where cryotic temperatures were not reached in situ. Applying a single linear regression model across all substrate types assumes homogeneous conductive behavior. For example, in coarse, air-filled felsenmeer, conductive gradients may be strongly nonlinear and influenced by advective processes [67]. Therefore, it should be interpreted qualitatively as indicating that any cryotic layer, if present, lies well below the reach of the probe, rather than as literal depths. These extrapolated values are not used for model calibration; instead, our conclusions focus on the observed prevalence and spatial clustering of failed tests as an indicator of low testability in such terrain.

This issue was considerably compounded by the limited number of sensors, which could be submerged at any given time. During the initial field design period, we anticipated that at the very least, the full length of the probe would be submerged at most herbaceous CAS. However, due to encountering buried felsenmeer at surprisingly shallow depths beneath some of the organic soils present at herbaceous CAS, this was not the case. As a result, this method was further limited by lowered data resolution.

5.3.2 | Model

This model is subject to the same limiting factors as all other models, in that any number of discrete training sites in a heterogeneous landscape cannot be comprehensive of the characteristics of the overall landscape. This is especially problematic in the Ogilvie Mountains, where the testability of the landscape proved to be just as heterogeneous as the ground thermal state. We initially anticipated that our CAS tests would reach no significant depth in the felsenmeer class and unanimously succeed in the herbaceous class, but the results were far more variable. Although the herbaceous class was the only class to produce in situ cryotic temperatures, greater depths were achieved in the felsenmeer class than were originally anticipated because of an unexpected variety of soil profile depths.

As noted by Léger et al. [33], permafrost investigations are frequently biased toward readily accessible sites. A similar accessibility bias is present in the training dataset used in this study. Extensive areas of the study region were too steep or unstable to be safely accessed, thereby limiting spatial coverage. In addition, logistical and time constraints resulted in a disproportionate concentration of sampling near the valley fronts, with comparatively less representation deeper down the fetch.

Pearson's correlation analysis and VIF testing for multicollinearity indicated that elevation was the only statistically significant predictor of testability among the environmental variables considered. Although this result is robust within the context of the data, we believe that it is still an oversimplification and constitutes a limitation of the P_{TEST} model. The model predicts low testability at high elevations, where felsenmeer and barren ridgetop are the dominant landcover types, and high testability at low elevations, where substrate is soft and organic. Essentially, elevation is functioning as a proxy for soil development. Because soft soil development is necessary for testing at any meaningful depth, this relationship is a practical utility for the model. However, soil development is driven by a number of complex controls, which are not captured by elevation alone.

5.3.2.1 | Model Comparison Results

5.3.2.1.1 | Comparison of CAS Sampling and P_{TEST} Model With Bonnaventure et al.. It is more challenging to compare the results of CAS sampling to the Bonnaventure et al. [58] model because it maps probability of permafrost presence rather than thermal state. Individual CAS therefore cannot be

said to strictly agree or disagree with the model, but can instead be evaluated in relation to the probability predicted at that location. The Bonnaventure et al. [58] model is also based on older calibration data and should be interpreted here as a broader historical and conceptual benchmark, rather than as a direct representation of present-day near-surface permafrost conditions. This comparison is retained because it remains one of the few existing local permafrost model products available for the study area at an appropriate spatial scale.

In both WS01 and WS02, zones of low testability (0%–25%) overlap strongly with high modeled permafrost probabilities, averaging 80.0% and 88.1%, respectively. By contrast, the highest-testability zones (75%–100%), which are concentrated mainly in valley bottoms, correspond to lower average modeled permafrost probabilities (62.9% in WS01 and 59.6% in WS02), despite several CAS in these settings recording cryotic temperatures in situ. This likely reflects the limited ability of the broader Bonnaventure et al. [58] model to capture local cold-air drainage and SBI effects [49]. Moderate permafrost probabilities also overlap substantially with moderate testability (25%–75%), reinforcing that the terrain where permafrost conditions are most uncertain is also where field validation is least straightforward. An important caveat is that P_{TEST} is mapped at 2-m resolution, whereas the Bonnaventure et al. [58] surface is 30 m. The coarser grid smooths fine-scale slope, substrate, and snow controls on testability, so some apparent mismatches likely reflect scale effects rather than true disagreement. In this sense, the scale mismatch is itself informative, highlighting that coarse-resolution model uncertainty and low field testability tend to co-occur.

5.3.2.1.2 | Comparison of CAS Sampling and P_{TEST} Model With Garibaldi et al.. The Garibaldi et al. [53] model is a TTOP model, which was calibrated using the localized temperature networks in WS01 and WS02. It also considers the influence of cold air drainage and SBIs, which are well understood to impact permafrost distribution in the study area [49]. It is also more recent to the time of CAS sampling. Although it predicts much more heterogeneous permafrost distribution in WS01 than in WS02, it is still largely in agreement with the results of sampling.

It is important, however, to distinguish between the physical interpretation of TTOP and the operational way it is used here. In an equilibrium sense, TTOP values above 0°C are not physically indicative of permafrost. Nevertheless, near-thaw positive TTOP conditions remain useful for identifying terrain where equilibrium-based models may underestimate lingering or ecosystem-buffered permafrost in disequilibrium environments, particularly where thaw response is delayed relative to recent atmospheric forcing. This issue has also been identified in recent hybrid modeling work in boreal terrain, where equilibrium TTOP approaches underpredicted permafrost extent unless calibrated against field observations [76]. In this study, the purpose of examining the near-thaw TTOP range was therefore not to define a true permafrost class, but to highlight terrain where thermal ambiguity and low field testability are most likely to co-occur.

Similar to the Bonnaventure et al. [58] model, areas more certain to be underlain by permafrost by the Garibaldi et al. [53] model intersect with test failures in both valleys. These zones largely cover high elevation felsenmeer slopes and ridgetops. This relationship may be due to the negative temperature anomalies associated with felsenmeer, wherein voids between clasts facilitate strong convective heat losses [67]. Although it is unideal when testability is low, it is less problematic in areas where certainty about permafrost presence is higher.

Tables 5 and 6 together clarify the central issue identified in this study. The overlap analysis in Table 5 shows that near-thaw TTOP conditions are concentrated mainly within the moderate P_{TEST} classes, and that this relationship remains broadly consistent under a wider sensitivity threshold, indicating that the association is not simply an artifact of threshold choice. This suggests that the terrain in which permafrost is most thermally sensitive is also the terrain where field validation is most difficult, likely because these areas combine thicker snow, higher soil moisture, organic-rich substrates, and coarse or unstable surface materials that both warm the near-surface thermal regime and hinder probe penetration. The confusion-matrix metrics in Table 6 reinforce this interpretation by showing that, although the Bonnaventure et al. [58] model has the highest overall accuracy and sensitivity, its zero specificity indicates a strong tendency to overpredict permafrost presence. The Garibaldi et al. [53] TTOP model is somewhat more balanced but still favors permafrost presence, whereas P_{TEST} provides the most even trade-off between sensitivity and specificity, supporting its value as a tool for identifying where permafrost model validation is most and least feasible in complex mountain terrain. These metrics should still be interpreted cautiously, however, because the small number of CAS lacking near-surface permafrost makes specificity particularly sensitive to a limited number of misclassifications.

5.3.2.1.3 | Recommendations for Future Work. This study has illustrated several challenges in the ability to test for permafrost in complex mountainous environments, primarily centered around substrate penetrability and site accessibility. The following section outlines suggestions for future research in this environment or other challenging periglacial terrain.

We believe that WS01 and WS02 are relatively reflective of the environments surrounding the Dempster Highway in the Ogilvie Mountains, and the combination of thermal heterogeneity and difficulty in testing is cause for concern. There is still no baseline of spatiotemporally consistent information about ground thermal state in this area, which drives considerable uncertainty about the future of the Dempster Highway and other critical infrastructure.

However, the pre-existing network of GTNs in the study area did provide us with long series data on MAGST across considerable distances, elevations, and land cover types. Creating and expanding networks such as this one could provide considerable benefit to permafrost research. Although MAGST cannot be considered the ultimate determinant of permafrost presence or absence at a site, these data are still a useful indicator. Deployment of GTNs and air temperature sensors at this scale and density is also significantly more cost and labor-efficient than deployment of boreholes at the same scale. These values can not only be used to identify zones of climatic resilience (i.e., areas where insulative vegetation is reducing permafrost thaw)

[35], but also to pinpoint areas where change is occurring more rapidly. A focus on the distribution and variations of ALT could be used to interpolate more responsive areas, which are more immediately vulnerable.

As described in previous sections, the ground thermal profiling probe used in this study produced limited results due to the spacing of the individual thermistors. Although the challenges for future research regarding probe design remain, it would be beneficial to attempt a similar study where there is greater vertical resolution of sensors.

Limited field data collection time and resources resulted in a smaller number of tested sites than would be preferred to clarify a strong predictor of testability, and future studies should examine more complex environmental drivers. This could be achieved with a higher resolution of CAS samples and a more complex assessment of different environmental variables, especially in zones where the P_{TEST} model identified what we consider to be "moderate" probability (25%–75%). These future tests would improve the model significantly.

6 | Conclusions

This study was focused on two central goals. The first was to explore the distribution of permafrost in two mountain valleys in the Ogilvie Mountains, and the second was to examine permafrost testability as a concept in the context of model validation. Although the issue of model validation has been discussed in previous literature, no other studies have attempted to quantify permafrost testability as a variable. This is also the first systematic attempt to ground-truth the study area for permafrost. Both the ground thermal profiling and P_{TEST} methodologies used for these goals are transferable to other studies. Forty-nine CAS were sampled during the field campaign between the two mountain valleys of interest. Of these, 36 were successful tests because the probe was able to reach a minimum of 45-cm B.D.

The study used these results to attempt to retroactively validate two localized permafrost models. The models were the probability model by Bonnaventure et al. [58] and the TTOP model by Garibaldi et al. [53], with the CAS results being in good agreement with both. This provides a positive outlook for the knowledge gap being addressed here. Both models were calibrated using a more localized data set and performed well against validation tests.

A model predicting the likelihood of conducting a successful permafrost test (P_{TEST}) in the terrain was generated using the data collected at the CAS. Elevation was determined to be the only significant predictor of test success via a logistic regression analysis. According to the model, most of the landscape falls within two polarized categories: extremely low likelihood (0%–25%) or extremely high (75%–100%). However, midslope elevations fall within a more moderate category (25%–75%) and warrant further testing.

The results of this research illustrate that understanding permafrost distribution in thermally complex environments, such as in mountains and in the discontinuous zone, is challenging. These environments are the most immediately vulnerable to climate change and represent the highest degree of uncertainty surrounding distribution, which is likely to continue impacting infrastructure under predicted warming scenarios. As climate change progresses, permafrost uncertainty will only increase. Therefore, it is critical that future studies continue to examine testability and apply validation to distribution models.

Acknowledgments

We would like to acknowledge that this research was conducted on the traditional territory of the Tr'ondëk Hwëch'in First Nation and thank them for their ongoing support of our research. We also thank the Yukon Territorial Government for giving us permission to conduct fieldwork in the territory (Research License # 6800-20-1143). We offer our sincere appreciation to our field assistants, S. MacLean, M. Codd, and S. Lamoureux, for their support in data collection, and to K. Welsh for his assistance in figure design. We thank the University of Lethbridge for supporting the programs and workspaces necessary to complete this research. Finally, we would like to thank the Natural Sciences and Research Council of Canada (NSERC) and the Northern Scientific Training Program (NSTP) for funding the fieldwork portion of this research.

Funding

This work was supported by the University of Lethbridge, the Natural Sciences and Engineering Research Council of Canada and the Northern Scientific Training Program.

Data Availability Statement

Data are available upon request to the corresponding author.

References

1. E. A. G. Schuur, J. Bockheim, J. G. Canadell, et al., "Vulnerability of Permafrost Carbon to Climate Change: Implications for the Global Carbon Cycle," *Bioscience* 58, no. 8 (2008): 701–714, https://doi.org/10.1641/b580807.

2. D. Streletskiy, O. Anisimov, and A. Vasiliev, "Permafrost Degradation," In *Snow and Ice-Related Hazards, Risks and Disasters*, (2015): 303–344, https://doi.org/10.1016/b978-0-12-394849-6.00010-x.

3. V. Masson-Delmotte, M. Schulz, A. Abe-Ouchi, et al., "Information From Paleoclimate Archives," in *Climate Change 2013: The Physical Science Basis. Contribution of Working Group I to the Fifth Assessment Report of the Intergovernmental Panel on Climate Change*, ed. T. F. Stocker, D. Qin, G.-K. Plattner, et al. (Cambridge University Press, 2013), 383–464.

4. W. Haeberli, C. Guodong, A. P. Gorbunov, and S. A. Harris, "Mountain Permafrost and Climatic Change," *Permafrost and Periglacial Processes* 4, no. 2 (1993): 165–174, https://doi.org/10.1002/ppp.3430040208.

5. T. Kohler, M. Giger, H. Hurni, et al., "Mountains and Climate Change: A Global Concern," *Mountain Research and Development* 30, no. 1 (2010): 53–55, https://doi.org/10.1659/mrd-journal-d-09-00086.1.

6. E. A. Schuur, A. D. McGuire, C. Schädel, et al., "Climate Change and the Permafrost Carbon Feedback," *Nature* 520, no. 7546 (2015): 171–179.

7. C. R. Burn, J. O. Moore, B. O'Neill, et al., "Permafrost Characterization of the Dempster Highway, Yukon and Northwest Territories," (2015).

8. J. Hjort, O. Karjalainen, J. Aalto, et al., "Degrading Permafrost Puts Arctic Infrastructure at Risk by Mid-Century," *Nature Communications* 9, no. 1 (2018): 5147, https://doi.org/10.1038/s41467-018-07557-4.

9. Z. Yang, W. Fang, L. Xia, et al., "Warming Increases Methylmercury Production in an Arctic Soil," *Environmental Pollution* 214 (2016): 504–509, https://doi.org/10.1016/j.envpol.2016.04.069.

10. W. Haeberli, Y. Schaub, and C. Huggel, "Increasing Risks Related to Landslides From Degrading Permafrost Into New Lakes in De-Glaciating Mountain Ranges," *Geomorphology* 293 (2017): 405–417, https://doi.org/10.1016/j.geomorph.2016.02.009.

11. T. C. Lantz and S. V. Kokelj, "Increasing Rates of Retrogressive Thaw Slump Activity in the Mackenzie Delta Region, N.W.T., Canada," *Geophysical Research Letters* 35, no. 6 (2008): L06502, https://doi.org/10.1029/2007gl032433.

12. W. Dobinski, "Permafrost," *Earth-Science Reviews* 108, no. 3–4 (2011): 158–169, https://doi.org/10.1016/j.earscirev.2011.06.007.

13. A. Bartsch, T. Strozzi, and I. Nitze, "Permafrost Monitoring From Space," *Surveys in Geophysics* 44, no. 5 (2023): 1579–1613, https://doi.org/10.1007/s10712-023-09770-3.

14. C. R. Duguay and A. Pietroniro. "Remote Sensing in Northern Hydrology: Measuring Environmental Change," In *Geophysical monograph*, American Geophysical Union, (2005), https://doi.org/10.1029/gm163.

15. A. Kääb, "Remote Sensing of Permafrost-Related Problems and Hazards," *Permafrost and Periglacial Processes* 19, no. 2 (2008): 107–136, https://doi.org/10.1002/ppp.619.

16. S. Westermann, C. R. Duguay, G. Grosse, and A. Kääb, "Remote Sensing of Permafrost and Frozen Ground," in *Remote Sensing of the Cryosphere*, ed. M. Tedesco (Wiley-Blackwell, 2014), 307–344, https://doi.org/10.1002/9781118368909.ch13.

17. J. Obu, S. Westermann, A. Bartsch, et al., "Northern Hemisphere permafrost map based on TTOP modelling for 2000–2016 at 1 km^2 scale," *Earth-Science Reviews* 193 (2019): 299–316.

18. T. Zhang, J. A. Heginbottom, R. G. Barry, and J. Brown, "Further Statistics on the Distribution of Permafrost and Ground Ice in the Northern Hemisphere," *Polar Geography* 24, no. 2 (2000): 126–131, https://doi.org/10.1080/10889370009377692.

19. J. Heginbottom, "Permafrost Mapping: A Review," *Progress in Physical Geography* 26, no. 4 (2002): 623–642.

20. K. Gisnås, B. Etzelmüller, C. Lussana, et al., "Permafrost Map for Norway, Sweden and Finland," *Permafrost and Periglacial Processes* 28, no. 2 (2017): 359–378.

21. K. Henry and M. Smith, "A Model-Based Map of Ground Temperatures for the Permafrost Regions of Canada," *Permafrost and Periglacial Processes* 12, no. 4 (2001): 389–398, https://doi.org/10.1002/ppp.399.

22. S. Vegter, P. P. Bonnaventure, S. Daly, and W. Kochtitzky, "Modelling Permafrost Distribution Using the Temperature at Top of Permafrost Model in the Boreal Forest Environment of Whatì, NT," *Arctic Science* 10 (2024): 455–475, https://doi.org/10.1139/AS-2023-0010.

23. B. Etzelmüller, "Recent Advances in Mountain Permafrost Research," *Permafrost and Periglacial Processes* 24, no. 2 (2013): 99–107, https://doi.org/10.1002/ppp.1772.

24. S. Gruber, "Derivation and Analysis of a High-Resolution Estimate of Global Permafrost Zonation," *Cryosphere* 6, no. 1 (2012): 221–233, https://doi.org/10.5194/tc-6-221-2012.

25. M. A. Walvoord and B. L. Kurylyk, "Hydrologic Impacts of Thawing Permafrost—A Review," *Vadose Zone Journal* 15, no. 6 (2016): 2016–2001.

26. M. K. Woo, D. L. Kane, S. K. Carey, and D. Yang, "Progress in Permafrost Hydrology in the New Millennium," *Permafrost and Periglacial Processes* 19, no. 2 (2008): 237–254.

27. D. Zou, L. Zhao, Y. Sheng, et al., "A New Map of Permafrost Distribution on the Tibetan Plateau," *Cryosphere* 11, no. 6 (2017): 2527–2542.

28. P. P. Bonnaventure and A. G. Lewkowicz, "Mountain Permafrost Probability Mapping Using the BTS Method in Two Climatically Dissimilar Locations, Northwest Canada," *Canadian Journal of Earth Sciences* 45, no. 4 (2008): 443–455.

29. S. Gruber and W. Haeberli, "Mountain Permafrost," in *Permafrost Soils*, Soil Biology, ed. R. Margesin, vol. 16 (Springer, 2009), 33–44, https://doi.org/10.1007/978-3-540-69371-0_3.

30. M. C. Garibaldi, P. P. Bonnaventure, N. C. Noad, and W. Kochtitzky, "Exploring the Impact of Surface Lapse Rate Change Scenarios on Mountain Permafrost Distribution in Four Dissimilar Valleys in Yukon, Canada," *Arctic Science* 10, no. 4 (2024a): 749–763, https://doi.org/10.1139/as-2023-0066.

31. J. Noetzli, L. U. Arenson, A. Bast, et al., "Best Practice for Measuring Permafrost Temperature in Boreholes Based on the Experience in the Swiss Alps," *Frontiers in Earth Science* 9 (2021): 607875.

32. V. Mühll, C. Hauck, and H. Gubler, "Mapping of Mountain Permafrost Using Geophysical Methods," *Progress in Physical Geography* 26, no. 4 (2002): 643–660, https://doi.org/10.1191/0309133302pp356ra.

33. E. Léger, B. Dafflon, Y. Robert, et al., "A Distributed Temperature Profiling Method for Assessing Spatial Variability in Ground Temperatures in a Discontinuous Permafrost Region of Alaska," *Cryosphere* 13, no. 11 (2019): 2853–2867, https://doi.org/10.5194/tc-13-2853-2019.

34. T. Rödder and C. Kneisel, "Influence of Snow Cover and Grain Size on the Ground Thermal Regime in the Discontinuous Permafrost Zone, Swiss Alps," *Geomorphology* 175 (2012): 176–189.

35. Y. L. Shur and M. T. Jorgenson, "Patterns of Permafrost Formation and Degradation in Relation to Climate and Ecosystems," *Permafrost and Periglacial Processes* 18, no. 1 (2007): 7–19.

36. I. Shirley, Z. A. Mekonnen, H. M. Wainwright, et al., "Near-Surface Hydrology and Soil Properties Drive Heterogeneity in Permafrost Distribution, Vegetation Dynamics, and Carbon Cycling in a Sub-Arctic Watershed," *Journal of Geophysical Research: Biogeosciences* 127, no. 9 (2022): e2022JG006864.

37. M. C. Garibaldi, P. P. Bonnaventure, and S. F. Lamoureux, "Utilizing the TTOP Model To Understand Spatial Permafrost Temperature Variability in a High Arctic Landscape, Cape Bounty, Nunavut, Canada," *Permafrost and Periglacial Processes* 32, no. 1 (2021): 19–34.

38. Y. Yi, J. S. Kimball, R. H. Chen, et al., "Characterizing Permafrost Active Layer Dynamics and Sensitivity to Landscape Spatial Heterogeneity in Alaska," *Cryosphere* 12, no. 1 (2018): 145–161, https://doi.org/10.5194/tc-12-145-2018.

39. G. Strandberg and P. Lind, "The Importance of Horizontal Model Resolution on Simulated Precipitation in Europe – From Global to Regional Models," *Weather and Climate Dynamics* 2, no. 1 (2021): 181–204, https://doi.org/10.5194/wcd-2-181-2021.

40. S. V. Daly, P. P. Bonnaventure, and W. Kochtitzky, "Influence of Ecosystem and Disturbance on Near-Surface Permafrost Distribution, Whatì, Northwest Territories, Canada," *Permafrost and Periglacial Processes* 33 (2022): 339–352, https://doi.org/10.1002/ppp.2160.

41. E. J. Stockton, C. R. Burn, M. Idrees, F. Calmels, and K. Elmer, "Monitoring Ground Temperatures in Permafrost Along the Dempster Highway, Yukon and NWT," In 18th International Conference on Cold Regions Engineering and 8th Canadian Permafrost Conference, (2019): 92–101. American Society of Civil Engineers.

42. M. C. Peel, B. L. Finlayson, and T. A. McMahon, "Updated World Map of the Köppen-Geiger Climate Classification," *Hydrology and Earth System Sciences* 11, no. 5 (2007): 1633–1644, https://doi.org/10.5194/hess-11-1633-2007.

43. R. Frappier, D. Lacelle, and R. H. Fraser, "Landscape Changes in the Tombstone Territorial Park Region (Central Yukon, Canada) From

Multilevel Remote Sensing Analysis," *Arctic Science* 9, no. 4 (2023): 838–855.

44. M. A. Brideau, A. Bevington, A. G. Lewkowicz, and D. Stead, "Engineering Geology, Electrical Resistivity Tomography and Displacement Monitoring of the Dawson City Landslide, Yukon," In 68th Canadian Geotechnical Conference, Quebec, Canada, Paper (Vol. 616), (2015).

45. D. Streletskiy, B. K. Biskaborn, S. Smith, J. Noetzli, G. Viera, and P. Schoeneich, "Strategy and Implementation Plan 2016-2020 for the Global Terrestrial Network for Permafrost (GTN-P)," Strategy and Implementation Plan 2016-2020 for the Global Terrestrial Network for Permafrost (GTN-P), (2017).

46. D. Lacelle, M. St-Jean, B. Lauriol, et al., "Burial and Preservation of a 30,000 Year Old Perennial Snowbank in Red Creek Valley, Ogilvie Mountains, Central Yukon, Canada," *Quaternary Science Reviews* 28, no. 27–28 (2009): 3401–3413.

47. J. Throop, A. G. Lewkowicz, and S. L. Smith, "Climate and Ground Temperature Relations at Sites Across the Continuous and Discontinuous Permafrost Zones, Northern Canada," *Canadian Journal of Earth Sciences* 49, no. 8 (2012): 865–876.

48. N. C. Noad and P. P. Bonnaventure, "Spatiotemporal Variability of Surface-Based Temperature Inversions in High-Latitude Northcentral Yukon Valleys Utilizing a Dense Network of Elevation Transects," *Arctic, Antarctic, and Alpine Research* 58, no. 1 (2026): 2614790.

49. N. C. Noad and P. P. Bonnaventure, "Surface Temperature Inversion Characteristics in Dissimilar Valleys, Yukon Canada," *Arctic Science* 8 (2022): 1320–1339, https://doi.org/10.1139/as-2021-0048.

50. A. Duk-Rodkin, "Surficial Geology, Dawson, Yukon Territory, 1:250,000," (1996).

51. A. Duk-Rodkin, "Glacial Limits Map of Yukon," Indian & Northern Affairs Canada/Department of Indian & Northern Development: Exploration & Geological Services Division, Geoscience Map 1999–1992, (1999).

52. H. M. French, *The Periglacial Environment* (John Wiley & Sons, 2017).

53. M. C. Garibaldi, P. P. Bonnaventure, N. C. Noad, and W. Kochtitzky, "Modelling Air, Ground Surface and Permafrost Temperature Variability Across Four Dissimilar Valleys, Yukon, Canada," *Arctic Science* 10 (2024b): 611–629, https://doi.org/10.1139/as-2023-0067.

54. N. C. Noad and P. P. Bonnaventure, "Examining the Influence of Microclimate Conditions on the Breakup of Surface-Based Temperature Inversions in Two Proximal but Dissimilar Yukon Valleys," *Canadian Geographies/Géographies Canadiennes* 68, no. 3 (2023): 323–339, https://doi.org/10.1111/cag.12886.

55. R. D. Şerban, H. Jin, M. Şerban, et al., "An Observational Network of Ground Surface Temperature Under Different Land-Cover Types on the Northeastern Qinghai–Tibet Plateau," *Earth System Science Data* 16, no. 3 (2024): 1425–1446.

56. J. Heginbottom, "*Canada, permafrost*: Canada Map Office," (1995).

57. H. B. O'Neill, S. A. Wolfe, and C. Duchesne, "New Ground Ice Maps for Canada Using a Paleogeographic Modelling Approach," *Cryosphere* 13, no. 3 (2019): 753–773, https://doi.org/10.5194/tc-13-753-2019.

58. P. P. Bonnaventure and A. G. Lewkowicz, "Permafrost Probability Modeling Above and Below Treeline, Yukon, Canada," *Cold Regions Science and Technology* 79 (2012): 92–106.

59. P. P. Bonnaventure and S. F. Lamoureux, "The Active Layer: A Conceptual Review of Monitoring, Modelling Techniques and Changes in a Warming Climate," *Permafrost and Periglacial Processes* 37, no. 3 (2013): 352–376, https://doi.org/10.1177/0309133313478314.

60. M. Idrees, C. R. Burn, J. Moore, and F. Calmels, "Monitoring Permafrost Conditions Along the Dempster Highway," In 7th Canadian Permafrost Conference: Proceedings of a Conference Held, (2015): 20–23.

61. H. B. O'Neill, C. R. Burn, and S. V. Kokelj, "Field Measurements of Permafrost Conditions Beside the Dempster Highway Embankment, Peel Plateau, NWT," In Proceedings from Conference: GEOQuébec, (2015).

62. J. Brown, K. M. Hinkel, and F. E. Nelson, "The Circumpolar Active Layer Monitoring (Calm) Program: Research Designs and Initial Results," *Polar Geography* 24, no. 3 (2000): 166–258, https://doi.org/10.1080/10889370009377698.

63. P. P. Bonnaventure, S. F. Lamoureux, and E. A. Favaro, "Over-Winter Channel Bed Temperature Regimes Generated by Contrasting Snow Accumulation in a High Arctic River," *Permafrost and Periglacial Processes* 28, no. 1 (2017): 339–346.

64. M. W. Smith and D. W. Riseborough, "Climate and the Limits of Permafrost: A Zonal Analysis," *Permafrost and Periglacial Processes* 13, no. 1 (2002): 1–15, https://doi.org/10.1002/ppp.410.

65. R. G. Way and A. G. Lewkowicz, "Environmental Controls on Ground Temperature and Permafrost in Labrador, Northeast Canada," *Permafrost and Periglacial Processes* 29, no. 2 (2018): 73–85.

66. S. A. Harris and D. E. Pedersen, "Thermal Regimes Beneath Coarse Blocky Materials," *Permafrost and Periglacial Processes* 9 (1998): 107–120.

67. H. Juliussen and O. Humlum, "Thermal Regime of Openwork Block Fields on the Mountains Elgåhogna and Sølen, Central-Eastern Norway," *Permafrost and Periglacial Processes* 19, no. 1 (2008): 1–18, https://doi.org/10.1002/ppp.607.

68. Y. Sawada, M. Ishikawa, and Y. Ono, "Thermal Regime of Sporadic Permafrost in a Block Slope on Mt. Nishi-Nupukaushinupuri, Hokkaido Island, Northern Japan," *Geomorphology* 52, no. 1–2 (2003): 121–130, https://doi.org/10.1016/s0169-555x(02)00252-0.

69. R. G. Way and A. G. Lewkowicz. "Investigations of Discontinuous Permafrost in Coastal Labrador With DC Electrical Resistivity Tomography," In *Proceedings of GéoQuebec: 68th Canadian Geotechnical Conference and 7th Canadian Permafrost Conference. Quebec City, Canada*, (2015): 8.

70. J. E. Holloway and A. G. Lewkowicz, "Half a Century of Discontinuous Permafrost Persistence and Degradation in Western Canada," *Permafrost and Periglacial Processes* 31, no. 1 (2020): 85–96.

71. A. G. Lewkowicz and M. Ednie, "Probability Mapping of Mountain Permafrost Using the BTS Method, Wolf Creek, Yukon Territory, Canada," *Permafrost and Periglacial Processes* 15, no. 1 (2004): 67–80.

72. K. Isaksen, R. S. Ødegård, T. Eiken, and J. L. Sollid, "Composition, Flow and Development of Two Tongue-Shaped Rock Glaciers in the Permafrost of Svalbard," *Permafrost and Periglacial Processes* 11, no. 3 (2000): 241–257.

73. M. J. Noh and I. M. Howat, "The Surface Extraction From TIN Based Search-Space Minimization (SETSM) Algorithm," *ISPRS Journal of Photogrammetry and Remote Sensing* 129 (2017): 55–76.

74. J. Jenness, "Topographic Position Index (tpi_jen.avx) Extension for ArcView 3.x, v. 1.3a," Jenness Enterprises (2006), http://www.jennessent.com/arcview/tpi.htm.

75. M. Kuhn, "Building Predictive Models in R Using the Caret Package," *Journal of Statistical Software* 28 (2008): 1–26.

76. P. P. Bonnaventure, S. MacLean, N. C. Noad, and M. C. Garibaldi, "A Statistical-Process Hybridized Approach to Modeling Permafrost Distribution in a Boreal Wetland Ecosystem, Whatì, NT, Canada," *Permafrost and Periglacial Processes* (2026): 1–19, https://doi.org/10.1002/ppp.70037.

77. A. B. Schetselaar and C. R. Burn. "Increases in Highway Maintenance Costs in a Permafrost Environment Undergoing Climate Change, Yukon, Canada," In Proceedings of the 12th International Conference on Permafrost, (2024): 373–381, Ottawa, ON: International Permafrost Association.

78. S. Gruber and W. Haeberli, "Permafrost in Steep Bedrock Slopes and Its Temperature-Related Destabilization Following Climate Change," *Journal of Geophysical Research: Earth Surface* 112 (2007).

79. M. Pavoni, J. Boaga, F. M. Wagner, A. Bast, and M. Phillips, "Characterization of Rock Glaciers Environments Combining Structurally-Coupled and Petrophysically-Coupled Joint Inversions of Electrical Resistivity and Seismic Refraction Datasets," *Journal of Applied Geophysics* 215 (2023): 105097.

80. K. Krainer, D. Bressan, B. Dietre, et al., "A 10,300-Year-Old Permafrost Core From the Active Rock Glacier Lazaun, Southern Ötztal Alps (South Tyrol, Northern Italy)," *Quaternary Research* 83, no. 2 (2015): 324–335.

81. K. Merz, H. Maurer, L. Rabenstein, T. Buchli, S. M. Springman, and M. Zweifel, "Multidisciplinary Geophysical Investigations Over an Alpine Rock Glacier," *Geophysics* 81, no. 1 (2016): WA147–WA157.

82. S. Monnier, C. Camerlynck, and F. Rejiba, "Ground Penetrating Radar Survey and Stratigraphic Interpretation of the Plan du Lac Rock Glaciers, Vanoise Massif, Northern French Alps," *Permafrost and Periglacial Processes* 19, no. 1 (2008): 19–30.

83. X. Fan, Y. Wang, F. Niu, et al., "Environmental Characteristics of High Ice-Content Permafrost on the Qinghai–Tibetan Plateau," *Remote Sensing* 15, no. 18 (2023): 4496.

84. H. M. French, *The Periglacial Environment*, 3rd ed. (Wiley, 2007).

85. B. Cao, T. Zhang, Q. Wu, Y. Sheng, L. Zhao, and D. Zou, "Brief Communication: Evaluation and Inter-Comparisons of Qinghai–Tibet Plateau Permafrost Maps Based on a New Inventory of Field Evidence," *Cryosphere* 13 (2019a): 511–519, https://doi.org/10.5194/tc-13-511-2019.

86. S. Hachem, C. R. Duguay, and M. Allard, "Comparison of MODIS-Derived Land Surface Temperatures With Ground Surface and Air Temperature Measurements in Continuous Permafrost Terrain," *Cryosphere* 6, no. 1 (2012): 51–69, https://doi.org/10.5194/tc-6-51-2012.

87. M. Langer, S. Westermann, M. Heikenfeld, W. Dorn, and J. Boike, "Satellite-Based Modeling of Permafrost Temperatures in a Tundra Lowland Landscape," *Remote Sensing of Environment* 135 (2013): 12–24, https://doi.org/10.1016/j.rse.2013.03.011.

88. D. Luo, H. Jin, S. S. Marchenko, and V. E. Romanovsky, "Difference Between Near-Surface Air, Land Surface and Ground Surface Temperatures and Their Influences on the Frozen Ground on the Qinghai-Tibet Plateau," *Geoderma* 312 (2018): 74–85, https://doi.org/10.1016/j.geoderma.2017.09.037.

89. S. Westermann, M. Langer, and J. Boike, "Spatial and Temporal Variations of Summer Surface Temperatures of High-Arctic Tundra on Svalbard—Implications for MODIS LST-Based Permafrost Monitoring," *Remote Sensing of Environment* 115, no. 3 (2011): 908–922.

90. M. Guglielmin, "Ground Surface Temperature (GST), Active Layer and Permafrost Monitoring in Continental Antarctica," *Permafrost and Periglacial Processes* 17, no. 2 (2006): 133–143, https://doi.org/10.1002/ppp.553.

91. J. Batbaatar, A. R. Gillespie, R. S. Sletten, et al., "Toward the Detection of Permafrost Using Land-Surface Temperature Mapping," *Remote Sensing* 12, no. 4 (2020): 695, https://doi.org/10.3390/rs12040695.

92. S. Westermann, T. Østby, K. Gisnås, T. V. Schuler, and B. Etzelmüller, "A Ground Temperature Map of the North Atlantic Permafrost Region Based on Remote Sensing and Reanalysis Data," *Cryosphere* 9, no. 3 (2015): 1303–1319, https://doi.org/10.5194/tc-9-1303-2015.

93. R. S. Ødegård, K. Isaksen, T. Eiken, and J. L. Sollid, "MAGST in Mountain Permafrost, Dovrefjell, Southern Norway, 2001–2006," in *Ninth International Conference on Permafrost, University of Alaska Fairbanks*, vol, 29 (2008): 1311–1315.

94. C. R. Burn and C. A. S. Smith, "Observations of the "Thermal Offset" in Near-Surface Mean Annual Ground Temperatures at Several Sites Near Mayo, Yukon Territory, Canada," *Arctic* 41, no. 2 (1988): 99–104.